Occurrence and transition probabilities of Omega and High-over-Low blocking in the Euro-Atlantic region

Carola Detring[1,2], Annette Müller[1], Lisa Schielicke[1], Peter Névir[1], and Henning W. Rust[1]

[1]Institut für Meteorologie, Freie Universität Berlin, Germany
[2]Meteorologisches Observatorium Lindenberg - Richard-Aßmann-Observatorium, Deutscher Wetterdienst, Germany

Correspondence: Carola Detring (carola.detring@dwd.de)

Abstract. Stationary, long-lasting blocked weather patterns can lead to extreme conditions such as anomalously high temperatures or heavy rainfall. The exact locations of such extremes depend on the location of the vortices that form the block. There are two main types of blocking: ~~(~~i) a *High-over-Low* block with a high located poleward of ~~a single low and (~~an isolated low and ii) an *Omega* block with two lows that lie ~~south east and south west~~ south-east and south-west of the blocking high on the Northern hemisphere. In this work, we will ~~introduce~~ refine a novel method based on the kinematic vorticity number and the point vortex theory that allows to distinguish between these two blocking types. Based on the National Center for Environmental Prediction - Department of Energy (NCEP-DOE) Reanalysis 2 data, we study the trends of the occurrence probability and the onset, offset, and transition probabilities of *High-over-Low* and *Omega* blocking in the 30-year period from 1990 to 2019 in ~~two regions on~~ the Northern Hemisphere (90°W-90°E~~and~~) and in the Euro-Atlantic sector (40°W-30°E)~~, we study the trends of the occurrence probability and the onset, offset, and transition probabilities of *High-over-Low* and *Omega* blocking~~. First, we use logistic regression to investigate ~~the~~ long-term changes of blocking probabilities ~~depending on~~ for full years, seasons and months. ~~On a yearly basis, our results show only small changes over the 30 years. However, analysing the trends on a monthly basis we find large differences in the occurrence probabilities with significant increases over the 30 year period in February, March and August and a significant decrease in December. The increases can mainly be attributed to an increasing probability~~ While trends are small for annual values, changes in occurrence probability are more prominent and also more diverse when broken down to seasonal and monthly resolution. A three-state multinomial regression describing the occurrence of *Omega* ~~blocks. Second~~and *High-over-Low* blocking reveals different trends for both types. Additionally, we use ~~a Markov model to calculate the~~ Markov models to describe transition probabilities for a two-state ~~model with an (~~*unblocked*~~and a~~ , *blocked*~~states, and~~) and a three-state ~~Markov model that additionally distinguishes between the specific blocking types (*High-over-Low*~~unblocked*~~and~~ , *Omega* ~~blocking. In a Markov modelthe transition probabilities depend only on the actual and the previous time step neglecting all previous time steps. Over the 30 year period, we~~ block, *High-over-Low* block) Markov model. We find the largest changes in transition probabilities in the summer season, where the transition probabilities towards *Omega* blocks significantly increase, while the unblocked state becomes less probable. ~~Hence, *Omega* blocks become more frequent and stable in summer at the expense of the other states.~~ Moreover, we show that *Omega* blocking is more likely to occur and to be more persistent than the *High-over-Low* blocking pattern.

1 Introduction

A blocking is a quasi-stationary, persistent large-scale atmospheric flow pattern that blocks the typical westerly flow and forces the jet and embedded pressure systems to bypass on its northern and southern sides (e.g. Rex, 1950). Blocks can last for several days up to weeks. Typically, a minimum blocking duration of 4 to 10 days is assumed (e.g. Rex, 1950; Pelly and Hoskins, 2003; Barriopedro et al., 2006, 2010; Barnes et al., 2011). ~~A block is~~ Northern hemisphere blocks are characterized by a steady ~~high pressure~~ high-pressure area accompanied by one ~~low pressure~~ low-pressure area southwards, called *High-over-Low*~~(dipole)~~, or by two ~~low pressure systems south- and eastwards~~ low-pressure systems southwest- and southeastwards of the high, called *Omega* block ~~(tripole) (see e.g. Bott, 2012; Woollings et al., 2018).~~ (see e.g. Bott, 2012; Woollings et al., 2018). Transitions between the different blocking types can be observed~~as e.g.~~ : An example is documented in Schielicke (2017, appendix A.3, Fig. A69) for summer 2010, where long-lasting blocking caused extreme heat and forest fires over Russia ~~. Due to its persistence~~ while downstream of the blocks "record-breaking" floods occurred in Pakistan (Hong et al., 2011; Schneidereit et al., 2012) . Due to their persistence and quasi-stationarity, blocks can determine the weather, especially temperature and precipitation ~~pattern~~patterns, in a large region over a long period of time. Depending on ~~its~~ their location, duration and intensity, these weather situations can have devastating, regional impacts ranging from heatwaves and droughts in the warm season to cold spells in winter and spring ~~(e.g. Pfahl and Wernli, 2012; Brunner et al., 2017, 2018; Russo et al., 2015).~~

~~Central European heatwaves, droughts and temperature records in the summer season made the headlines in recent years.In the past years, particularly in 2018 and 2019, a series of blocking led to exceptional, "unprecedented" drought conditions in the two consecutive summers (Hari et al., 2020).~~ (e.g. Pfahl and Wernli, 2012; Russo et al., 2015; Brunner et al., 2017, 2018; Hari et al., 2020) . Furthermore, the blocking type , i.e. *High-over-Low* or *Omega* ~~blocking situations that occurred in~~ block, determines the location of observed or expected extreme weather phenomena. For example, in June and July 2019~~caused widespread temperature records~~ , *Omega* blocking caused record-breaking temperatures far above 40°C at several locations in western and central Europe (Vautard et al., 2020), with an observed record temperature of 45.9°C in southern France ~~at 28 June 2019~~ (Henley et al., 2019) and 41.2°C in western Germany ~~on 25 July 2019~~ (Deutscher Wetterdienst, 2020, 2019; Bissolli et al., 2019). In ~~general, a block consists of a long lasting high together with one or two persistent low pressure areas, which can lead to contrary weather situations. For example, the *Omega* blocking that caused the persistent heatwave over Russia in June to August 2010 also led to "record-breaking" floods downstream in Pakistan (e.g. Hong et al., 2011). At the western flank of a quasi-stationary blocking over northern Europe in May /~~May and June 2018, an ~~unusual~~ unusually high number of slow-moving thunderstorms caused heavy rain rates and flash floods in large parts of western and central Europe ~~(Mohr et al., 2020).~~ located at the western flank of a quasi-stationary blocking over northern Europe (Mohr et al., 2020). Hence, we expect that the knowledge of the blocking type can help to better estimate the regions which will be impacted.

~~A~~ In order to classify blocking types, the point vortex model can be used. This idealized model gives one conceptual explanation of ~~atmospheric blocking is based on an idealized point vortex model. It was introduced by Obukhov et al. (1984) and further studied in Kuhlbrodt and Névir (2000); Müller and Névir (2014); Müller et al. (2015). It is~~ the quasi-stationarity of atmospheric blocking (see e.g. Obukhov et al., 1984; Kuhlbrodt and Névir, 2000; Müller and Névir, 2014; Müller et al., 2015)

. It represents a Lagrangian formulation of the vorticity equation with vortices ~~conceived~~ pictured as "particles" ~~, where,~~ with circulation being conserved for each vortex~~, the circulation is conserved.~~

[1]. The motion of a set of point vortices is determined by their circulations and the intervortical distances only, see e.g. ~~Aref (1979); Newton (2001)~~Aref (1979) and Newton (2001). Hirt et al. (2018) statistically ~~confirm~~ confirmed the theory of Müller et al. (2015) that the *Omega* blocking pattern can be regarded as a three point vortex system (~~tripole) with the anticyclonic point vortex, i. e. the high, located on the poleward side of two cyclonic point vortices. In case~~ or tripole). If these three vortices ~~lie on the vertices of a equilateral triangle and if~~ form an equilateral triangle (i.e. arranged as in Fig. 1(b)) with the sum of ~~all three circulations is~~ their circulations being zero, the point vortex system ~~*moves*~~ moves westwards opposing the typical westerly ~~wind~~ flow of the mid-latitudes. Stationarity ~~of the the vortex system is explained if both speeds are identical~~is achieved when the magnitude of the westerly flow matches the translation speed of the point vortex system. Analogously, a *High-over-Low* block can be described by a point vortex pair (~~dipole)~~ or dipole) of zero total circulation that moves westward ~~. This concept is summarized in~~ (see Fig. 1~~. Applying the point vortex theory allows for the identification and location of each high and the low pressure systems separately. Furthermore, this leads to the possibility to classify and analyse the two blocking states *High-over-Low* and *Omega* blocking types. It should be noted, that this discrete perspective is contrary to~~ (d)). The point vortex concept allows to classify the ~~explanation of the blocking based on Rossby-waves as studied by e.g. Tung and Lindzen (1979). Further authors, Tyrlis and Hoskins (2008), Berrisford et al. (2007), Altenhoff et al. (2008) describe the onset of general blockings with the Rossby wave breaking. Using this method based on point vortices provides the opportunity to identify the high and low pressure systems separately. This leads to the first question motivating this present work: Can we find a method to automatically distinguish between the two atmospheric blocking types~~ blocking state into *High-over-Low* ~~and~~ or *Omega*~~blocks?~~ , as well as to determine the location and intensity of each vortex associated with the block in gridded data. It is now possible to observe transitions between the blocking states within a longer blocking period.

The ~~identification of blocking depends on the specific definition and method used. Therefore, blocking climatologies can differ with respect to frequency and location of blocking (e.g. Barriopedro et al., 2010). Although different methods yield different results, they agree in two general aspects: blocking maxima are observed in the North Pacific and North Atlantic-European region, and higher blocking numbers occur in boreal winter compared to the summer season (e.g. Pinheiro et al., 2019). However, larger variability is observed on a block-to-block basis (Pinheiro et al., 2019) and from year-to-year (Davini et al., 2012)~~ .

~~The~~ numerical prediction of blocking onset and persistence, i.e. the transition from zonal to blocked flow and vice versa, is still a challenge. However, it is still important to study these transitions; Ferranti et al. (2015) showed that medium-range ensemble forecasts in the Euro-Atlantic region are less skillful in these situations. ~~For a better understanding, transitions between different large-scale weather regimes have been studied by cluster analyses and the application of Markov chains by e.g. Spekat et al. (1983); Egger (1987); Vautard et al. (1990); Kimoto and Ghil (1993). A Markov model describes the probabilities~~

[1]It should be noted, that the discrete point vortex perspective is contrary to the explanation of blocking based on Rossby-waves as studied by, e.g., Tung and Lindzen (1979). Further authors, Tyrlis and Hoskins (2008), Berrisford et al. (2007), Altenhoff et al. (2008) describe the onset of general blocks with the Rossby wave breaking.

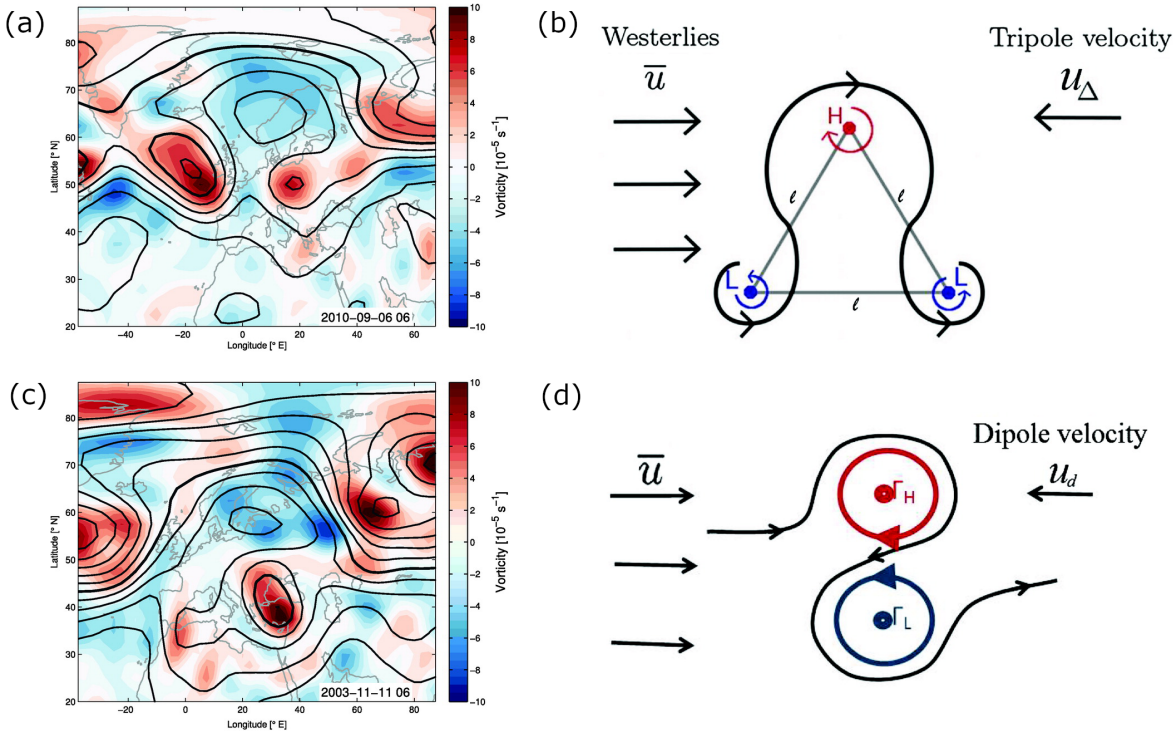

Figure 1. Application of point vortex theory to two distinct atmospheric blocking types:(a),(b): *Omega* blocking (c),(d): *High-over-Low* blocking.(a) and (c): Two exemplary blocking events observed at the 500 hPa level: Displayed is the relative vorticity (colour-shaded) and contours of geopotential height in 8 dm intervals (bold contour represents 552 dm). (b),(d): Illustration how the corresponding blocking can be realized in the point vortex model. Figure is adapted from Hirt et al. (2018, their figure 2, published under the terms of the Creative Commons Attribution License (http://creativecommons.org/licenses/by/4.0/)) with upper right figure taken from Müller et al. (2015). The point vortex systems become stationary if the ~~westerlies~~ typical westerly flow of the mid-latitudes and the propagation speed of the dipole/tripole ~~velocities~~ point vortex systems are of equal magnitude.

~~of~~ One way to describe the probability of transitions between the states of a system ~~. For this purpose, only the present state is taken into account. Hence,~~ is the use of discrete-state Markov models. These models describe the probability of the system in a future state as dependent on the present state only; the future state ~~becomes~~ is hence independent of all previous states ~~except of the current one (e.g. Grewal et al., 2019).~~ (e.g. Grewal et al., 2019). Cluster analyses followed by Markov chains have been used to describe the transitions between different large-scale weather regimes by several authors, e.g. Spekat et al. (1983); Egger (1987); Vautard et al. (1990); Kimoto and Ghil (1993). Spekat et al. (1983) distinguishes between zonal, mixed and meridional weather regimes in central Europe. They found relatively long residence times within the regimes of 5 to 7 days and relatively low daily transition probabilities of 5 % to 11 % between the regimes. However, to the best of our knowledge, the transition between different blocking types within the same blocked period, i.e. the transition from *Omega* ~~and~~

to *High-over-Low* ~~blocks, and the unblocked state~~ and vice versa, has not been studied so far~~on a sub-daily, 6-hourly time scale . On this data basis, we will analyse the occurrence of the different blocking types, tackling the second question if blocking occurrence probabilities undergo long-term changes and if these changes depend on season or month? The third question arises: Do onset (formation), offset (decay) or transition probabilities from one blocking type to another undergo long-term changes? Do these changes depend on season or month? Davini and D'Andrea (2020)~~ . While blocked periods last for at least five days, transitions occur on a smaller time scale and higher temporal-resolution data (e.g. 6 hours) thus needs to be analyzed.

Due to their socio-economic relevance, it is of common interest to study and determine blocking climatologies and trends. It is also observed that the identification of blocking depends on the specific definition and method used (e.g. blocking indices). Blocking climatologies can, furthermore, differ with respect to the frequency and location of blocking (e.g. Barriopedro et al., 2010) , and also often depend on the model data (Barnes et al., 2014). Although different methods yield different results, they agree in two general aspects: blocking maxima are observed in the North Pacific and North Atlantic-European region, and higher blocking numbers occur in boreal winter compared to the summer season, but the details of the climatologies depend on the blocking identification method used (e.g. Fig. 6 in Pinheiro et al., 2019). However, larger variability among methods can be observed even when looking at individual blocking events (Pinheiro et al., 2019) and from year-to-year (Davini et al., 2012) . Davini and D'Andrea (2020) compare the blocking frequency for different regions using different models ~~. Analysing the linear trend~~ for the time period 1951-2017~~, also for seasons, the authors find a large spread among the different models and large dependencies on the region. Analysing the trend of the seasons, the authors find that~~ . Moreover, analysing seasonally resolved trends, they find a negative trend in blocking frequency for the Northern Hemisphere ~~the blocking trend is negative~~ in winter, and ~~positive~~ a positive trend in summer. Even though their results show a general decrease ~~of blocking frequency in~~ in blocking frequency for the future, the impact in some regions and seasons, e.g. the summer Ural blocking, might increase. ~~By investigating linear blocking trends in the time period 1980–2012 Barnes et al. (2014) show that the blocking trends also depend on the blocking indices and the models. The authors~~ Barnes et al. (2014) find no general evident increase in blocking over the Northern Hemisphere~~. But~~ , but they further show that the results depend on the ~~regions, seasons~~ region, season and also on the analyzed time period. ~~There~~ For example, there are significant seasonal increases for some regions, such as Asia ~~(DJF)~~ in boreal winter and the North Atlantic ~~(JJA). Furthermore~~in boreal summer. Additionally, Cheung et al. (2013) confirm a strong dependence of the blocking frequency on the seasons. Their results indicate that the strength of blocking events, in terms of intensity and extension, is stronger in winter and weaker in summer. But they also state that the impact of summer blocks might be higher.

~~To answer the three questions, Can we find a method to automatically distinguish between the two atmospheric blocking types~~ In this work, we study climatologies and annually, seasonally and monthly resolved trends of blocking occurrence probabilities with a novel strategy: blocking type classification based on point vortex theory followed by a description of occurrence and transition probabilities with logistic regression and Markov models. Furthermore, we will extend the existing literature on trends in blocking occurrence by the aspect of blocking types. Since these blocking types are connected to different typical regions of high-impact weather, their long-term occurrence trends are of general interest. Hence, we refine the

fluid-dynamically-based method developed in Hirt et al. (2018) to classify blocking into *High-over-Low* and *Omega* ~~blocks?~~ and use logistic regression and Markov models to address the following research questions:

1. Do blocking occurrence probabilities undergo long-term changes? Do these changes depend on season or month?

2. Do onset (formation), offset (decay) or transition probabilities from one blocking type to another undergo long-term changes? Do these changes depend on season or month?

~~the~~ The work is structured as follows. First, we shortly describe the data set and variables ~~that will be used for our analysis in Section~~in Section 2. In ~~Section 3, we will~~ Sections 3.1 to 3.4, we explain the steps of our ~~method~~ identification and classification strategy in more detail~~: This includes the identification of blocking events (Section 3.1) and their properties (Section 3.2). Moreover, the decision process for the blocking types – *High-over-Low* or *Omega* block – is explained in Section3.3. We use a subset of the blocking data (Section 3.4) in order to analyse the Euro-Atlantic region with respect to the evolution and transition probabilities of blocking. The statistical methods used in~~ . Section 3.5 gives a short overview of logistic and multinomial regression for the analysis of occurrence probabilities~~(logistic regression) and for the transition probabilities (Markov processes) are explained in Sections 3.5 and 3.6. The results will be presented in Section~~. Section 3.6 introduces discrete-state Markov processes for the analysis of transition probabilities between blocking types. Results follow in Section 4 and discussed subsequently in Section 5. We close with a conclusion in Section ~~5. A final concise conclusion is given in Section~~ 6.

2 Data

We ~~used~~ use the NCEP-DOE Reanalysis 2 data set (Kanamitsu et al., 2002) for our analysis. The data has a grid spacing of $2.5° \times 2.5°$ on a regular latitude/longitude grid and is available every 6 hours. In our study, we used a period of 30 years from 1990 to 2019. We restricted the analysis to the 500 hPa level, a level where the divergence of the horizontal wind field is close to zero (Schielicke, 2017). This allows us to apply the principles of point vortex theory that requires ~~incompressible flow, i. e. a zero divergence. The variables used for this study were the~~ two-dimensional non-divergent flow. We use geopotential height and the horizontal wind components (U, V) at 500 hPa ~~. We will~~ to compare the blocking behaviour in two regions. The first region covers half the Northern Hemisphere from $90° W$ to $90° E$~~, and the~~ . The second region is a subset of this larger region covering the Euro-Atlantic area from $40° W$ to $30° E$.

3 Methods and ~~design of~~ study design

In the following we describe the ~~data preparation and the methodology for the probabilistic analysis of atmospheric blocking~~ . six steps of the analysis. Starting from the identification of blocked latitudes (Step 1, section 3.1) and the calculation of blocking properties with the trapezoid method (Step 2, section 3.2) to classification of blocking into *Omega* and *High-over-Low* types (Step 3, section 3.3), followed by the choice of the region of interest (Step 4, section 3.4). Finally, we introduce logistic and

multinomial regression to model occurrence probabilities (Step 5, section 3.5), as well as Markov models to describe transition probabilities (Step 6, section sec:markov). The steps are summarized in Fig. 2.

3.1 Step 1. Identification of instantaneous blocked longitudes (IBLs) and blocking events

In the first step, we use the *Blocking* plugin (Richling et al., 2015) of the *Freva* system (Freie Universität Berlin Evaluation System, see Freva, 2017; Kadow et al., 2021) to calculate the so-called instantaneous blocking index. This index is a binary 1d blocking index that determines instantaneous blocked longitudes (IBLs) for every time step of a data series. The IBL was developed by Tibaldi and Molteni (1990) and identifies blocks in terms of gradients of the geopotential height with regard to a central reference blocking latitude (CRBL). While the CRBL is fixed to $50° N$ in the original work, the *Freva* blocking plugin uses a modification (after Barriopedro et al., 2010) that allows for a longitudinally-dependent, temporally-varying CRBL in accordance to the climatological stormtrack. A blocking is identified if the geopotential height gradients on the northern (GHGN) and on the southern (GHGS) side of the CRBL satisfy the following criteria (following Richling et al., 2015):

$$GHGS = \frac{Z(\phi_M) - Z(\phi_S)}{\phi_M - \phi_S} > 0 \frac{gpm}{°N} \quad \text{: corresponding to an easterly directed flow} \tag{1}$$

$$GHGN = \frac{Z(\phi_N) - Z(\phi_M)}{\phi_N - \phi_M} < -10 \frac{gpm}{°N} \quad \text{: similar to a westerly flow} > 8 \text{ m/s} \tag{2}$$

where Z is the geopotential height at 500 hPa and the latitudes are given as $\phi_S = (\phi_C - 0.5\delta_\phi) + \Delta$, $\phi_M = (\phi_C + 0.5\delta_\phi) + \Delta$ and $\phi_N = (\phi_C + 1.5\delta_\phi) + \Delta$. Here, δ_ϕ is set to 15° latitude. Here, the spatio-temporally varying CRBL ϕ_C is determined based on the 30-year climatology (1990-2019) of the 500 hPa geopotential height field. In order to capture blocking that are not directly located at the CRBL, a possible shift Δ to the north and south is set to 10° latitude. For each time step, we obtain a binary value for all longitudes (either 1: blocked or 0: unblocked). For more details on the method and the specific configurations used in the analysis see the Supplementary Material and Richling et al. (2015).

Prior to the blocking classification, the time series of IBLs is post-processed in the following manner: First, we identify *blocking events* as simply-connected points of IBL = 1 in the time-longitude field. Then we chose events with a minimum duration of five days, i.e. 20 time steps, and a spatial extent of at least 15 degrees

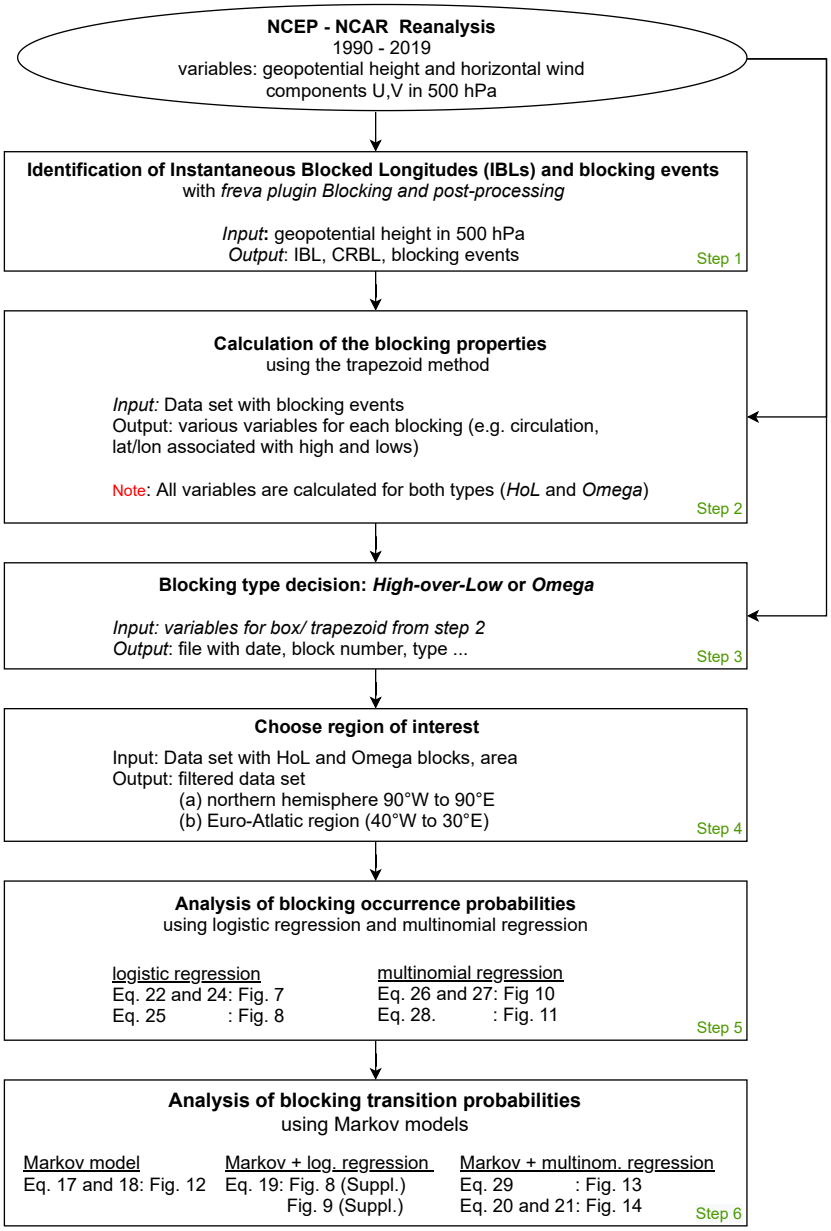

Figure 2. Structure diagram of the individual steps of the evaluation as explained in section 3.

~~longitudes~~longitude. We only consider Northern Hemisphere blocks in the longitudinal range of $90° W$ to $90° E$ and north of about $45° N$. Note, that ~~we can have~~ two blocking events can exist at the same time in different parts of the area ~~. If this caseoccurs, the state of the first block is used for the analysis~~since the region is very large. In this case, only the first blocking is considered for the subsequent analysis. Further blocking events are discarded, since only one state can be ~~assigned~~ used per time step~~for the analysis. The second blocking event is discarded.~~.

3.2 Step 2. Calculation of the blocking properties with the trapezoid method

~~The~~

Based on the blocking event list ~~derived in~~ from step 1~~will be used to~~, we now search for blocking patterns in the corresponding ~~NCEP Reanalysis fields . For this purpose we applied~~ NCEP-DOE Reanalysis fields with the trapezoid method (Müller et al., 2015; Hirt et al., 2018) ~~that is able~~ to detect *High-over-Low* and *Omega* blocking patterns~~using~~. This approach uses aspects of flow kinematics to identify the vortices, as well as point vortex theory to determine blocking properties and to classify the blocking type. ~~The idea behind the trapezoid method is that, in~~ In a regular latitude-longitude projection, a *High-over-Low* block ~~resembles~~ can be outlined by a rectangle (or box) surrounding the high and the low~~while~~; an *Omega* block ~~resembles~~ instead, can be outlined by a trapezoidal shape, where the two lows form the broader base of the trapezoid and the high its smaller top. By assigning specific parts of the trapezoid or box to each low and high, we are able to determine the properties (circulation, location of vortex center) of the associated vortices (cf. Fig. 3 of Müller et al., 2015). The trapezoid method as it is used here is based on the method introduced in Hirt et al. (2018) with slight modifications~~and the~~. The reader is referred to their publication for more details. We will give a brief overview ~~over method here~~of the method in the following.

The highs and lows are detected by an analysis of the kinematics of the flow. ~~Therefor~~Therefore, we use the dimensionless kinematic vorticity number $W_k = \|\mathbf{\Omega}\|/\|\mathbf{S}\|$ (Truesdell, 1953, 1954), which compares the local ~~rates of rotation~~ rotation-rate $\|\mathbf{\Omega}\|$ and ~~strain~~ strain-rate $\|\mathbf{S}\|$ at each grid point. Here, $\mathbf{\Omega} = [\nabla\mathbf{v} - (\nabla\mathbf{v})^{\mathbf{T}}]/\mathbf{2}$ and $\mathbf{S} = [\nabla\mathbf{v} + (\nabla\mathbf{v})^{\mathbf{T}}]/\mathbf{2}$ denote the ~~antisymmetric~~ anti-symmetric and symmetric components of the velocity gradient tensor $\nabla\mathbf{v}$ that describes the kinematic flow properties around a point. In our case, $\mathbf{v} = (u, v)$ represents the horizontal wind vector.

For two-dimensional flow ~~, $W_k = \sqrt{\zeta^2}/\sqrt{2(\partial_x u)^2 + 2(\partial_y v)^2 + (\partial_x v + \partial_y u)^2}$ with ∂_x, ∂_y indicating partial derivatives in x-, y-direction and $\zeta = \partial_x v - \partial_y u$ is the vertical vorticity.~~ in spherical coordinates with longitude $\phi \in [0, 2\pi]$, latitude $\theta \in [-\pi/2, \pi/2]$, and Earth's radius R, the kinematic vorticity number $W_k = |\zeta|/|D|$ is proportional to the magnitude of the horizontal deformation, where

$$|D| = \frac{1}{R}\sqrt{2\left(\frac{1}{\cos\theta}\frac{\partial u}{\partial \phi}\right)^2 + 2\left(\frac{\partial v}{\partial \theta}\right)^2 + \left(\frac{1}{\cos\theta}\frac{\partial v}{\partial \phi} + \frac{\partial u}{\partial \theta}\right)^2} \quad . \tag{3}$$

The vertical component of relative vorticity ζ (called vorticity from now on) is given as

$$\zeta = \frac{1}{R\cos\theta}\frac{\partial v}{\partial \phi} - \frac{1}{R}\frac{\partial u}{\partial \theta} \quad . \tag{4}$$

For the calculation of ~~$\|\mathbf{\Omega}\|$, $\|\mathbf{S}\|$ and~~ W_k, we use the two-dimensional, horizontal wind components of the ~~NCEP~~ NCEP-DOE reanalysis data set at the 500 hPa level. A vortex is then defined as region of $W_k > 1$, i.e. as an area where the rotation-rate prevails over the strain-rate (see Schielicke et al., 2016; Schielicke, 2017, for further insight and more atmospheric applications). ~~On the other hand,~~ Otherwise, the W_k values at all grid points ~~with values of~~ where $W_k \leq 1$ are set to zero to obtain a field of vortex patches. This field can then be multiplied with ~~some~~ another field of interest, for example the ~~vertical~~ vorticity field to get areas of positive and negative vorticity, i.e. cyclones and anticyclones on the Northern Hemisphere. In this field, we search for the anticyclone that lies closest to a ~~duration-weighted IBL~~*duration-weighted* IBL[2]. Inside a box bounded by this *duration-weighted* IBL$\pm 15°$ ~~longitudes~~ longitude and between $55°$N and $85°$N the grid point with the most negative circulation $\mathbf{P}_{max,neg}$ is identified first. The circulation of a grid point i is ~~given by~~ calculated as

$$\Gamma_i = \zeta_i A_i \ , \tag{5}$$

where ζ_i is the ~~vertical~~ vorticity at that grid point and A_i is the area associated with grid point i. It is negative/positive if the ~~vertical~~ vorticity is negative/positive. The circulation of the high Γ_H is calculated as the sum of all grid points N with negative circulation inside a radius of 1500 km around $\mathbf{P}_{max,neg}$ as

$$\Gamma_H = \sum_i^N \Gamma_i \quad \text{for } \Gamma_i < 0 \ . \tag{6}$$

The radius of 1500 km was chosen following Hirt et al. (2018) who did a sensitivity study to find the optimal radius that represents the circulation magnitude of the high. Therefore, Hirt et al. (2018) started with a smaller radius of 500 km around the high centroid and increased the size gradually by 250 km steps up to 3000 km. They observed, that the circulation magnitude stabilizes around a radius of 1500 km, which was then chosen as threshold (see Hirt et al., 2018, for more details). Moreover, the Rossby radius of deformation in a stably-stratified, dry high is indeed larger compared to aless stable low-pressure system because of the larger Brunt-Väisälä-frequency. This further supports the choice of 1500 km.

Similar to the definition of the circulation centroid of a vortex system in point vortex theory, the circulation centroid of the real, extended high is defined as (see also Hirt et al., 2018)

$$\mathbf{C}_H = \frac{\sum_i^N \Gamma_i \mathbf{x}_i}{\Gamma_H} \quad \text{for } \Gamma_i < 0 \ , , \tag{7}$$

where $\mathbf{x}_i$ is the horizontal coordinate vector of grid point i and N is defined as above. Note, that the (positive) circulation and the circulation centroid of a low are calculated in a similar way. The coordinates $(C_{H,x}, C_{H,y})$ of centroid $\mathbf{C}_H$ are finally used to define the rectangle that encloses the high by a fixed distance: $(C_{H,x} \pm 1500\,\text{km}, C_{H,y} \pm 1500\,\text{km})$ which accounts for the typical length scale of a high in the ~~midlatitudes~~ mid-latitudes and allows for some deviations from a pure circular shape. The rectangle, that encloses the high, is then extended equatorwards by steps of $2.5°$ ~~latitudes to obtain a~~ latitude up to $20°$N. These

[2]This means, that each IBL is assigned with the maximum number of time steps (duration) that this IBL is blocked. For each time step separately, each blocked IBL (either ~~"0"~~ 0 or ~~"1"~~ 1) is multiplied with its maximum duration and the associated longitude. This product is summed up and then divided by the sum of all IBL ~~durations~~ duration at this time step to get the *duration-weighted* IBL.

boxes are then compared to identify the box that minimizes the total circulation within the box. The total circulation is defined as the sum of the negative circulation associated with the high and the positive circulation associated with the low. However, only grid points with negative circulation northwards of the low centroid and positive circulation south of the high centroid are taken into account for the calculation of the total circulation. This box ~~shape approximates~~ outlines the *High-over-Low* configuration. At the same time, we search for a minimum of total circulation within a trapezoidal shape, which represents an *Omega* configuration. ~~Therefor, we enlarge the southern boundary of the step-wise changed~~ To this end, we increase the southern edge of the box symmetrically by steps of 2.5° longitudes (on each side) up to a total length of ~~the southern trapezoid boundary of~~ 2.5 times the east-west-length of the box around the high center. The northern boundary remains fixed and only grid points whose centers lie within the trapezoidal shape are counted. Again, only certain areas of the trapezoid are attributed to the high (everything north of the mean latitude of the low centers), to the western low (everything south and west of the high centroid) and the eastern low (everything south and east of the high centroid).

~~This~~ Point vortex theory is the basis for this pattern-like identification~~is based on the point vortex theory, which~~. It states that a system of two or three vortices moves westward if the sum of their circulations is zero, the high lies poleward of the low(s), and the ~~3-point-vortex-system~~ three-point-vortex-system forms an equilateral triangle (Müller et al., 2015). Note, that we determine the box associated with the *High-over-Low* pattern as well as the trapezoid with the *Omega* pattern for each time step separately. ~~Moreover, for each pattern~~ We derive a number of block properties, such as the circulations, ~~and~~ the latitude and longitude associated with the high and the lows (centroids) ~~are derived for later analysis~~for each pattern. The decision ~~,~~ ~~which~~ on the blocking type pattern ~~better fits, is done directly after the calculation of the trapezoid and box shape and is~~ is described in the following step 3.

3.3 Step 3. Blocking type decision: *High-over-Low* or *Omega* blocking

~~For the blocking type decision,~~ We inspect the relative vorticity in the area south of the circulation centroid of the high ~~around the~~ with coordinates (lon_H, lat_H) for the blocking type decision. To this end, a rectangle is centered around the coordinate $(lon_H, \overline{lat_L})$ where $\overline{lat_L}$ is the mean latitude of the ~~circulation centroids of the lows (trapezoidal shape derived in step2) is inspected as follows: A rectangle is centered around the longitude of the high centroid and mean latitude of the lows and split in 3~~ low centroids that are associated with the *Omega* block pattern at that time step. This rectangle has a latitudinal extend[3] of at least 10°. Its longitudinal extend is bound to the size of the trapezoid. We split this rectangle in three smaller rectangles where the middle one has a width of 25 degrees longitude and the two outer rectangles are limited by the outline of the trapezoid (see Fig.~~3a~~ 3(a))[4]. If the mean ~~vertical~~ vorticity inside the middle rectangle (Box 2 in Fig.~~3a) is higher than the mean vertical~~ 3(a)) is larger than the sum of the mean vorticity of all three rectangles~~together,~~, we define the time step ~~is defined~~ as *High-*

[3] More precisely, the latitude lat_{LW}, lat_{LE} of each cyclonic circulation centroid (low-pressure system) associated with the *Omega* block is determined. These latitudes are rounded to the latitude of the closest grid point. The rectangle then extends from $min(lat_{LW}, lat_{LE}) - 2.5°$ to $max(lat_{LW}, lat_{LE}) + 5°$. If $lat_{LW} = lat_{LE}$, then the height of the rectangle is 10° latitude.

[4] The middle box's width of 25 degrees has been carefully tested in Hirt et al. (2018). At this width, the identified number of *Omega* blocks in comparison to *High-over-Low* blocks were relatively stable. Moreover, the majority of the blocks remained in the same category while changing the box width by some degrees longitude. Hence, we decided to stick to this width in our analysis.

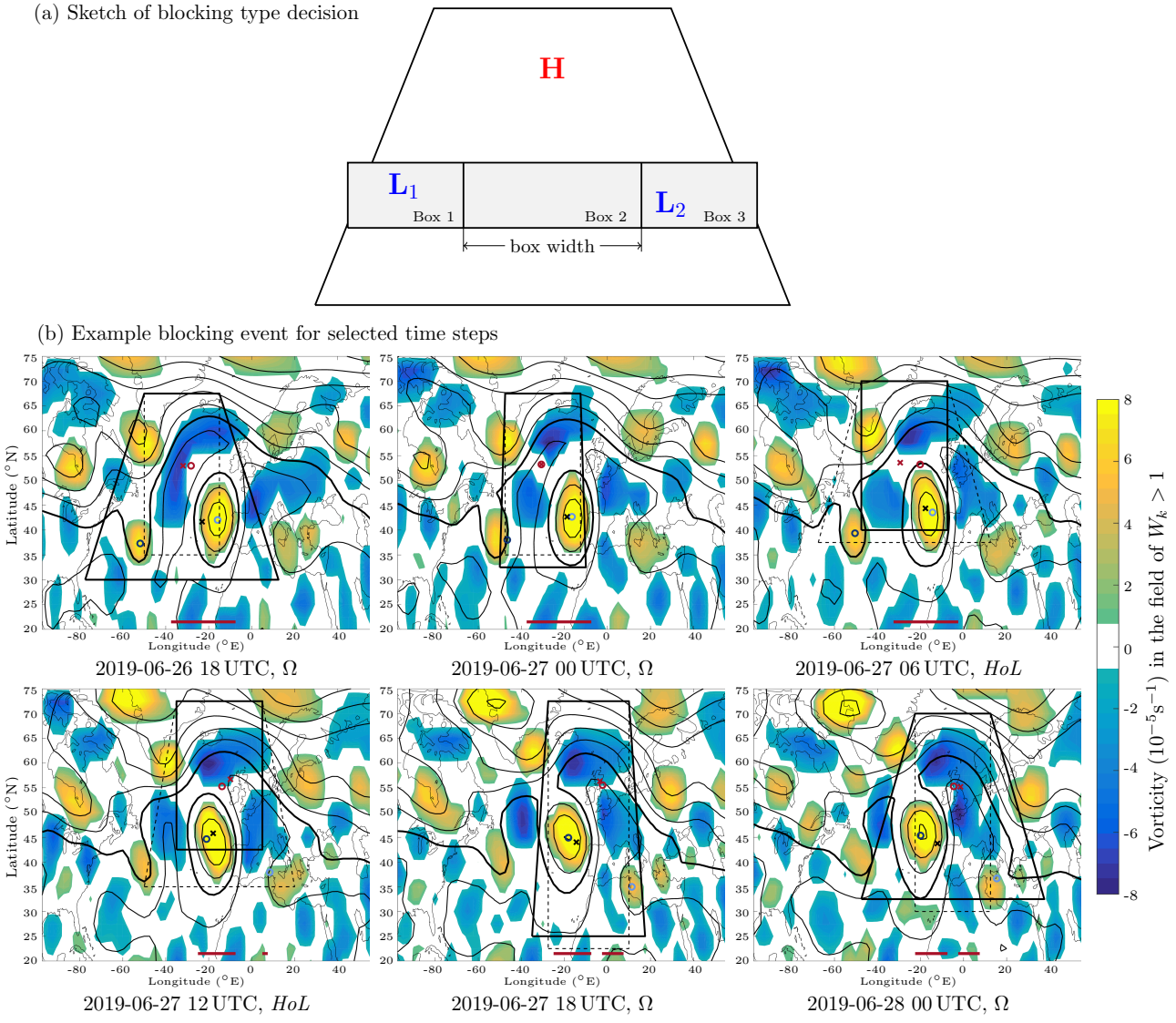

Figure 3. (a) Schematic representation of the blocking type decision based on the trapezoid method. The positive ~~vertical~~ relative vorticity is calculated for all three boxes, which lie on the mean latitude of the ~~low pressure~~ low-pressure areas (L_1, L_2). Depending on the magnitude of the mean ~~vorticty~~ vorticity in these three boxes, the decision between *High-over-Low* and *Omega* is made. (b) An example blocking event, observed at ~~26.~~ 26 June 2019, 18:00:00 UTC - ~~28.~~ 28 June ~~0~~ 2019, 00:00:00 UTC, is plotted for six time steps that include a transition between *Omega* and *High-over-Low* blocking states. Shaded areas represent the identified vortex field ($W_k > 1$) which is colored by relative vorticity (in $10^{-5}s^{-1}$; blue: anticyclonic; yellow: cyclonic). Black contours are isolines of geopotential height in ~~80~~8 ~~gpm~~ dm intervals (thick black contour is the ~~5840~~584 ~~gpm~~ dm isoline). The outline of the trapezoid/box is given for each time step, solid shape represent the identified shape; circles ~~(crosses)~~ are the circulation centroids of the identified high (red) and low(s) (blue) for the *Omega* ~~(~~pattern. In the same way, crosses are used for *High-over-Low* ~~)~~ pattern. The red bar(s) at the bottom of the figures shows the identified IBLs from Step 1. The figures were plotted with help of Matlab (2016) and coastlines were plotted with the built-in Matlab file *coast.mat*. The full time series is given in the Supplementary Material, see also steps 2 and 3.

over-Low block~~; otherwise the time step is defined~~ , otherwise as *Omega* ~~) block. Finally, we have~~ block. This results in a time series ~~of each blocking event that can contain~~ containing both blocking types ~~within~~ for a single blocking event (for an example see Fig.~~3b~~ 3(b) and the video in the Supplementary Material). This is a new addition to the trapezoid method in Hirt et al. (2018), who assigned a single blocking type to each whole blocking period. Finally, ~~the time series is once more checked for consistency: In our analysis,~~ a blocking event is expected to consist of the same anticyclone ~~. This is rather a Lagrangian view. Hence~~and we check if this assumption holds: In order to obtain configurations associated with the same high, we split ~~the blocking periods to~~ each blocking period into smaller periods, if ~~a certain *distance criterion* is breached: We assume that~~ the distance between the centroid locations of two highs in successive time steps (6 hours) is too large (*distance criterion*). We assume that these two highs represent the same system, if ~~their centroid locations differ less~~ the distance is smaller than 10 degrees latitude (≈ 1000 km in north-south direction) and ~~less~~ smaller than 15 degrees longitude (≈ 1000 km in west-east direction). ~~Although we allow~~ Otherwise, we assume that these two highs represent two different systems. This allows for slow motions of the blocks~~, these "large jumps"~~ ; "large jumps" in distances, however, would rather indicate that a different ~~high pressure~~ high-pressure system enters the configuration. ~~In order to obtain configurations associated with the same high, we split such periods to two or more smaller periods.~~ If the lifetime of one or both events ~~becomes less than 5~~ in the split period is shorter than five days, the event(s) is(are) removed from the analysis. ~~Of course this~~ This reduces the maximum duration of the blocking periods ~~,~~ but is also more consistent with following the ~~block~~ blocking as a system of vortices (instead of a weather regime that characterizes a larger region). This rather Lagrangian view on blocking differs from the Eulerian perspective we would get using only the instantaneous blocked longitudes to identify blocking.

~~At this point, our method differs from other blockingidentification methods that are solely based on indices. In~~ Note, that we follow mostly the method described in Hirt et al. (2018) who already tested the sensitivity of the trapezoid method regarding the choice of several parameters. We would like to refer the interested reader to their paper for more details. However, in order to better estimate the effect of the distance criterion that we introduce in this work, we did a number of experiments with different distances (see Table 1). ~~Our initial intent was~~ As we intent to bound the distance between high centroids in successive time steps by the typical synoptic-scale Rossby radius $L_D \approx 1000$ km~~. Hence~~, all experiments have distances which are close to this value. ~~For this paper, we will~~ In section 4, we present results for experiment E05 (see Table 1) with criterion $\Delta lat = 10° / \Delta lon = 15°$ (if not mentioned otherwise).

Table 1. Labeling of experiments with different distance criteria that are used to estimate the uncertainty of the blocking identification method. ~~Longitudes~~ Differences in longitude Δlon and ~~Latitudes~~ latitude Δlat are given in degrees.

Δlon: / Δlat:	11°	12°	13°	14°	15°	16°	17°	18°	19°
8°		E04			E25			E26	
10°	E14		E15		**E05**		E17		E18
12°		E27			E28			E06	

3.4 Step 4. Choose region of interest: Euro-Atlantic region and half Northern Hemisphere

~~The blocking data set derived after applying~~ Following step 1 to 3~~is composed of blocking events that occur~~ , we are left with blocking events occurring between $90° W$ and $90° E$ with a ~~life time~~ lifetime of at least ~~5~~ five days (= 20 time steps). ~~The detected high centers~~ High centroids lie in the mid-latitudes between about $44.5° N$ and $83° N$. To analyse blocking in Europe in more detail, we ~~separated this data set in a second~~ create a subset: the Euro-Atlantic sector ranging from $40° W$ to $30° E$. Since this is a subset of the larger blocking event list, blocks with ~~life times smaller than 5~~ lifetimes smaller than five days can occur in this region ~~. At~~ as at some point in their ~~life time, these blocks~~ lifetime, blocks might move in or out of the ~~Euro-Atlantic~~ Euro-Atlantic sector.

3.5 Step 5. Analysis of blocking occurrence probability using logistic regression

Logistic regression is designed to model probabilities ~~(~~p (with $0 \leq p \leq 1$) and is ~~an adequate model~~ thus adequate to describe blocking occurrence probabilities and their temporal changes for a system that can only yield two states: in our case *blocking* and *no-blocking* patterns. ~~The occurrence~~ Occurrence probabilities for a system with three possible states: *unblocked*~~and two distinct blocking states (~~, *Omega* and *High-over-Low*~~)~~, can be ~~analogously~~ analogously described with multinomial regression. Both are briefly reviewed here.

Logistic regression is a special case of generalized linear models (e.g., Wilks, 2011; Dobson and Barnett, 2008) designed to describe occurrence probabilities depending on a set of external influences (covariates). These covariates can be, for example, time in years as a proxy for climate change, the season or month of occurrence as a proxy for the seasonal cycle, or also large-scale atmospheric flow variables.

The setting can be viewed as a generalization to standard linear models. Let Y_t be a discrete random variable at discrete times t; observations of Y_t are denoted as y_t. The random variable Y_t describes the discrete states of a Markov chain. ~~The two-state model we~~ We begin our analyses with ~~,~~ the two-state model, that is based on these two states: *no blocking* (nB) and *blocking* (B)~~, observations~~ . Observations (coded in integers) can thus only be $y_t = 0$ for nB and $y_t = 1$ for B. The random variable Y_t follows a binomial distribution completely determined by the expectation value which gives the occurrence probability of the blocking event $E[Y_t] = Pr\{Y_t = 1\} = p_t$. The probability of the state *no blocking* is determined by the counter-probability $Pr\{Y_t = 0\} = 1 - p_t$.

Logistic regression describes the dependence of the blocking occurrence probability p_t at time t as a function of covariates $x_{l,t}$ using a log-odds (or logit) link-function

$$\text{logit}(p_t) = \ln\left(\frac{p_t}{1-p_t}\right) = \beta_0 + \Sigma_{l=1}^{L} \beta_l \, x_{l,t} \,, \tag{8}$$

with $l = 1, \ldots, L$ covariates $x_{l,t}$ observed simultaneously with observations y_t and β_l ~~are~~ being model parameters to be estimated based on iteratively reweighted least-squares (IRLS). Further details can be found, e.g., in Dobson and Barnett (2008); Wilks (2011). We use the function `glm()` from the package `stats` of the `R`-environment for statistical computing (R Core Team, 2018).

Rearranging Eq. (8) yields the following expression for the blocking occurrence probability at time t as a function of the covariates $x_{l,t}$:

$$p_t = \frac{1}{1+e^{-(\beta_0+\Sigma_{l=1}^{L}\beta_l x_{l,t})}}\,. \tag{9}$$

In some cases, the influence of one covariate $x_{i,t}$ dependents on the value of another covariate $x_{j,t}$ which can be introduced in a linear model as a so called *interaction* effect $x_{i,t}\,x_{j,t}$. Think of, for example, the change in blocking occurrence probability with years is dependent on the season, we are looking at. A simple example with *main effects* of two covariates and one *interaction* is

$$\mathrm{logit}(p_t) = \beta_0 + \beta_1\,x_{1,t} + \beta_2\,x_{2,t} + \beta_3\,x_{1,t}\,x_{2,t}\,. \tag{10}$$

In the notation for generalized linear models introduced by McCullagh and Nelder (1989) Eq. 10 reads

$$\mathrm{logit}(p_t) \sim x_{1,t} * x_{2,t} \sim x_{1,t} + x_{2,t} + x_{1,t} : x_{2,t}\,, \tag{11}$$

with $x_{i,t}$ denoting main effects, $x_{1,t} : x_{2,t}$ interaction effects and $x_{1,t} * x_{2,t}$ their ~~commonly used~~ combination. This notation assumes an offset (β_0) being present by default and a parameter β_i to be estimated for each term in the equation. Nota bene: in this notation, the symbols '$+$', ':' and '$*$' have special meanings, namely addition of a term in the predictor, interacting effects and combination of both, respectively~~.~~!

For more than two states, the model can be extended to multinomial logistic regression. We next consider a multinomial random variable Y_t with three states: ~~no blocking~~ *no blocking* (nB), *High-over-Low* (HoL) and *Omega* blocking (Ω). For the multinomial distribution, one probability, e.g. $Pr\{Y_t = nB\} = p_{nB,t}$, is set as reference and the other two $Pr\{Y_t = HoL\} = p_{HoL,t}$ and $Pr\{Y_t = \Omega\} = p_{\Omega,t}$ need to be estimated using

$$\ln\left(\frac{p_{HoL,t}}{p_{nB,t}}\right) \sim x_{1,t} + x_{2,t} + \ldots \tag{12}$$

$$\ln\left(\frac{p_{\Omega,t}}{p_{nB,t}}\right) \sim x_{1,t} + x_{2,t} + \ldots\,. \tag{13}$$

The remaining occurrence probability for ~~no blocking~~ *no blocking* can then be derived as $p_{nB,t} = 1-(p_{\Omega,t}+p_{HoL,t})$. We thus need to solve two regression equations simultaneously. This can be formulated in the framework of (vector) generalized linear models (VGLMs) (Yee, 2015). Parameter estimation is somewhat more cumbersome in this case~~and~~, realized using iteratively reweighted least squares ~~detailed in (Yee, 2015)~~and detailed in Yee (2015). Estimation is carried out using the function `vglm()` from the `R`-package `VGAM` (Yee, 2015). Confidence intervals (95%) are based on asymptotic normality of the estimator using an interval $[\hat{\theta} \pm 1.96\,\sigma_{\hat{\theta}}]$ around the estimator $\hat{\theta}$ with standard deviation $\sigma_{\hat{\theta}}$.

3.6 Step 6. Analysis of blocking transition probabilities using Markov models

We use Markov models with two and three states to describe transition probabilities between the states related to the different blocking types and the ~~no-blocking~~ *no-blocking* state. For both cases, there is thus a discrete set of possible states:

Two-state model: *blocked* (B) and *unblocked* (nB) states,

Three-state model: *High-over-Low* (HoL), *Omega* (Ω) and *unblocked* (nB) states.

The system evolves along a discrete time axis t and can switch between these discrete states. We obtain a *discrete-time Markov chain* on a finite state space. The underlying theory was developed by the Russian mathematician Andrey Andreyevich Markov~~(~~. For the translated original work see Markov (2006)~~).~~ .

Let Y_t be a sequence of discrete random variables denoting the possible states the Markov chain can be found in~~, e~~. E.g., $Y_t = i$ implies Y being in state i at time t~~, in~~ . In general $i \in \{1, 2, 3, \ldots, I\}$, here, $I = 2$ or $I = 3$ for the two-state-model or three-state-model, respectively. We speak of a transition when $Y_{t-1} = i$ changes to $Y_t = j$. Transitions from $Y_{t-1} = i \to Y_t = j$ are described with conditional probabilities which, in general, depend on the history of the process, i.e.

$$p_{ij,t} = P(Y_t = j \mid Y_{t-1} = i, Y_{t-2}, Y_{t-3}, \ldots)\,. \tag{14}$$

Formally, $Y_{t-1} = i \to Y_t = i$ is also called a transition from state i to itself. The Markovian assumption (or Markov property) requires these transition probabilities to depend only on the actual state and not the full history of the process

$$p_{ij,t} = P(Y_t = j \mid Y_{t-1} = i, Y_{t-2}, Y_{t-3}, \ldots) = P(Y_t = j \mid Y_{t-1} = i)\,. \tag{15}$$

This assumption makes handling these processes a lot easier. For *homogeneous* Markov chains, the transition probabilities are independent of external factors or time, i.e. $p_{ij,t} = p_{ij}$, otherwise we speak of a *non-homogeneous* Markov chain. The probability for finding the system at time t in state j, i.e. $Pr\{Y_t = j\}$, is determined by the transition probabilities p_{ij} from all states i into state j weighted with the probability $Pr\{Y_{t-1} = i)$ of finding the system in state i, thus

$$Pr\{Y_t = j\} = \sum_i Pr\{Y_t = j \mid Y_{t-1} = i\} Pr\{Y_{t-1} = i) = \sum_i p_{ij,t} Pr\{Y_{t-1} = i\}\,. \tag{16}$$

The simplest Markov Chain is a Bernoulli process consisting of two states~~, in our case~~. In our case, the two-statemodel with the states *no blocking* (nB) and *blocking* (B) ($i, j \in \{nB, B\}$) has the ~~two-state-model with *no blocking* (nB) and *blocking* (B) ($i, j \in \{nB, B\}$) with transition probabilities given in the~~ transition matrix

$$M_2 = \begin{pmatrix} p_{nB,nB} & p_{nB,B} \\ p_{B,nB} & p_{B,B} \end{pmatrix} \tag{17}$$

with transition probabilities $p_{nB,B} = Pr\{Y_t = B \mid Y_{t-1} = nB\}$. For the three-state-model (*High-over-Low~~blocking~~* blocking (HoL), *Omega* blocking (Ω) and *no-blocking* (nB), $i, j \in \{nB, HoL, \Omega\}$), the transition matrix is

$$M_3 = \begin{pmatrix} p_{nB,nB} & p_{nB,HoL} & p_{nB,\Omega} \\ p_{HoL,nB} & p_{Hol,HoL} & p_{HoL,\Omega} \\ p_{\Omega,nB} & p_{\Omega,HoL} & p_{\Omega,\Omega} \end{pmatrix}\,. \tag{18}$$

Transition probabilities are between 0 and 1 ($0 \leq p_{ij} \leq 1$) and rows sum up to unity, implying that the probability that any of the possible states i is reached at time $t + 1$ is one. Transition probabilities together with the probability distribution of Y_0 (initial distribution) fully describe the Markov chain.

Homogeneous (time-independent) Markov chains can be illustrated using a network diagram. Figure 4 shows an example with two states. The circles describe the different states and the arrows indicate the direction of the transition with the corresponding transition probability p_{ij}. In the homogeneous case, transition probabilities can be estimated from relative frequencies. A more general description of Markov chains and their matrices of transition probabilities can be found in Chap. 9.2 in Wilks (2011). More examples of atmospheric applications of (finite-state) Markov chains can be found in Gottwald et al. (2016, Chapt. 3.4). For further details on homogeneous Markov processes, see e.g. Baclawski (2008).

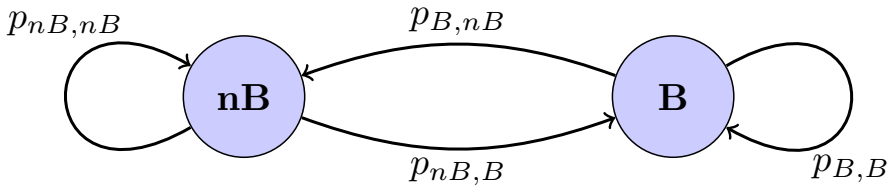

Figure 4. A general example of a network diagram of a homogeneous Markov chain with two states nB (*no blocking*) and B (*blocking*). Arrows indicate transitions and p_{ij} the associated transition probabilities between state i and j with $i, j \in \{nB, B\}$. After Baclawski (2008).

For a non-homogeneous (time-dependent) Markov-process, we use logistic regression to estimate time varying transition probabilities. For the two-state model with the two states *blocking* ($Y_t = B$) and *no blocking* ($Y_t = nB$), we describe transition probabilities changing with Year as

$$\text{logit}(P(Y_t = B \mid Y_{t-1})) \sim Y_{t-1} * \text{Year}\,, \tag{19}$$

using the notation for generalized linear models as well the parameter estimation strategies introduced above. This results in probabilities for blocking conditioned on being in an unblocked state $Pr\{Y_t = B \mid Y_{t-1} = nB\}$ and conditioned on being in a blocked state $Pr\{Y_t = B \mid Y_{t-1} = B\}$ varying in time. So do their counter probabilities $Pr\{Y_t = nB \mid Y_{t-1} = nB\} = 1 - Pr\{Y_t = B \mid Y_{t-1} = nB\}$ and $Pr\{Y_t = nB \mid Y_{t-1} = B\} = 1 - Pr\{Y_t = B \mid Y_{t-1} = B\}$. Analogously, we can describe time-varying (with Year and season (Seas) or month (Mon)) transition probabilities for the three-state model using multinomial logistic regression, setting the reference to $Pr\{Y_t = nB \mid Y_{t-1}\}$ and

$$\ln\left(\frac{Pr\{Y_t = HoL\} \mid Pr\{Y_{t-1}\}}{Pr\{Y_t = nB \mid Y_{t-1}\}}\right) \sim Y_{t-1} * \text{Year} * \text{Seas}\,, \tag{20}$$

$$\ln\left(\frac{Pr\{Y_t = \Omega\} \mid Pr\{Y_{t-1}\}}{Pr\{Y_t = nB \mid Y_{t-1}\}}\right) \sim Y_{t-1} * \text{Year} * \text{Seas}\,. \tag{21}$$

Probabilities for all transitions can be derived with the condition $Pr\{Y_t = HoL\}+Pr\{Y_t = \Omega\}+P\{Y_t = nB\} = 1$. For details on main and interaction effects with categorical terms in the predictor ~~, see Wilks (e.g., 2011); Dobson and Barnett (e.g., 2008)~~ see e.g. Wilks (2011) and Dobson and Barnett (2008).

4 Results

~~In~~

The results are divided into four subsections in order to answer the research questions ~~asked~~ posed in the introduction~~the results are divided into four subsections. First, we will study the uncertainties of the method and give~~ : 1. Do blocking occurrence probabilities undergo long-term changes? 2. Do onset, offset or transition probabilities between blocking types undergo long-term changes? In both cases, we ask if these long-term changes depend on season or month. We start with an overview of ~~the total number and duration of blocking for the chosen experiment settings.Then,~~ blocking properties and explore the uncertainty of the identification algorithm in Sect. 4.1. It follows a description of the temporal development of blocking occurrence probabilities for yearly, seasonal and monthly changes of the ~~two-states~~ two-state Markov model (*blocking, no blocking*) ~~are taken into account.In the third subsection the same analysis is done for three-states~~ in Sect. 4.2.1 and for the three-state Markov model (*no blocking, Omega, High-over-Low*) ~~. In the last part the~~ in Sec. 4.3. Section 4.4 discusses the transition probabilities of two and three states for the 30 year period~~are discussed in general. These transitions are also analyzed and shown with respect to their temporal evolution.~~ .

4.1 Uncertainty estimates of the identification method and general overview of ~~block~~ blocking properties

~~In order to better estimate the uncertainty of the identification method, we use a~~ A number of experiments with different distance criteria between the ~~high~~ high-pressure centroids of subsequent time steps allows to estimate the sensitivity of the identification method with respect to the distance criterion (see Table 1). ~~We will~~ The results of these sensitivity experiments are given as footnote to the results presented. The number of identified blocking turns out to be sensitive to the distance criterion with lower number for stricter (i.e. smaller) maximum distances.

Furthermore, we take a closer look at some general blocking properties such as ~~their~~ frequency and duration and their ~~number and how these are affected by~~ sensitivity to the distance criterion. Generally, the total number of blocks as well as the mean blocked days per year are lower for stricter distance criteria and increase almost linearly with relaxing the criterion (Fig.~~5b,c). Thereby, the longitudinal distance is the driving mechanism,~~ 5(b),(c)). The longitudinal distance has a higher impact, while a change in the latitudinal distance criterion only leads to slight differences (e.g. compare experiments E05, E28 and E25 in Fig.~~5b,c~~ 5(b),(c) which differ by 2° to 4° ~~latitudes~~latitude, but have the same longitudinal distance criterion).

In the 30-year period from 1990 to 2019 in the region $90°\,W$ to $90°\,E$, we detect a total of 389 blocks ($\approx$13 blocks per year) that lasted for five or more days (see Fig. 5~~a~~(a), blue columns) with an average of about 94 blocked days per year (92 ± 16 for all experiments). ~~For all considered~~ Over all experiments, we observe a mean ($\pm$ standard deviation) of 381 ± 52 blocks in total in this period (or 12.7 ± 1.7 blocks per year)~~, i. e. the variability of block numbers is about 14%. Out of~~ . 289 blocks (284 ± 40

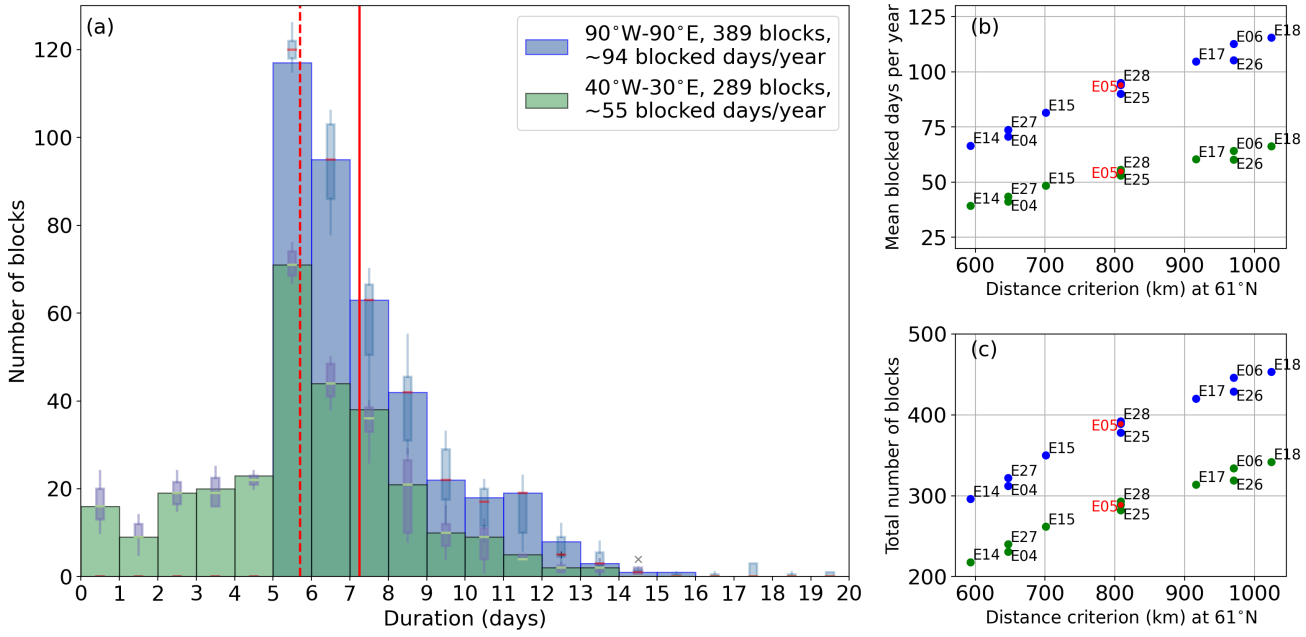

Figure 5. (a) Histogram of the duration of all blocking events in the period 1990-2019 for two selected regions. Blue (green) columns represent the region $90^\circ W$ to $90^\circ E$ ($40^\circ W$ to $30^\circ E$) for experiment E05 with a total of 389 identified blocks (289 blocks); red solid (dashed) vertical lines indicate the mean of this data set. Boxplots on top of the bars show the range of the identified block numbers given by different distance criteria (see Table 1). Boxes ~~indicate~~ show the ~~inner-quartile~~ interquartile range (IQR); whiskers ~~extends to~~ indicate 1.5 times ~~the inner-quartile range~~IQR; the ~~"~~"x"~~"~~" is an outlier (larger region). (b) Mean blocked days per year and (c) total number of identified blocks in the period 1990-2019 in dependence of the distance criterion. Here the distance criterion was calculated by the longitude criterion of the respective experiments at 61°N, which is the mean latitude of all identified highs.

blocks in total for all experiments) out of the 389 blocks ~~,~~ affected the Euro-Atlantic region ($40^\circ W$ to $30^\circ E$) ~~was affected by 289 blocks (284 ± 40 blocks in total for all experiments) for~~ for at least some of ~~the lifetime of the blocks~~ their lifetime with an average of about 55 blocked days per year (53 ± 9 for all experiments). Since the Euro-Atlantic blocks are a subset of the blocks that occur in the larger region, blocking lifetimes can be smaller than ~~5~~ five days. However, only 87 of the 289 blocks remained less than ~~5~~ five days in the Euro-Atlantic region, while the majority affected the region for 5 to 8 days (153 blocks, see Fig.~~5a~~ 5(a), green columns). Since blocks are observed to be quasi-stationary with usually low ~~travel~~ propagation speeds, the small number of short-lived blocks in the Euro-Atlantic region probably start or end close to the region boundaries and move either in or out of the region during their ~~life time~~lifetime. The mean duration of the blocks is 7.25 days for the larger region, and 5.70 days for the Euro-Atlantic region (red vertical lines in Fig.~~5a~~ 5(a)). Considering all experiments, the mean duration is 7.19 ± 0.30 days for $90^\circ W$ to $90^\circ E$, and 5.62 ± 0.15 days for $40^\circ W$ to $30^\circ E$, i.e. the variability in the mean duration is only about 1 time step (6 hours) between all considered experiments. The ~~inner-quartile~~ interquartile range (IQR, purple boxes

in Fig.~~5a~~ 5(a)) of the different experiments remains relatively consistent up to a duration of 8 days for the Euro-Atlantic region with $IQR = 5.3$ blocks per class. For this region, the largest disagreement between the experiments is found for blocks with a duration between 8 and 9 days with $IQR = 16.5$ blocks. Interestingly in the larger region, the lowest IQR of 4 blocks is found in the class with the highest block number with a duration between 5 and 6 days. In all other classes, the experiments differ more strongly with $IQR \approx 12$ blocks on average for lifetimes between 6 and 12 days. The number of blocks is ~~sensible~~ sensitive to the distance criterion (Fig.~~5c~~ 5(c)) which leads to splits of blocking events of the IBL-detected blocking periods into two or more smaller periods and can hence increase (or decrease, if the new periods are less than ~~5~~ five days) the overall number of blocks. In terms of averaged blocked days per year (Fig.~~5b~~ 5(b)), the standard deviations is 16 days for the larger region and 9 days for the smaller one. These values account for a fraction of 0.05, and 0.025, respectively, of additionally (or less) blocked days per year.

The temporal development of the annual blocking frequency and duration for the ~~half Northern Hemisphere and the~~ larger and the smaller Euro-Atlantic ~~sector~~ region is shown in Fig. 6.

~~In~~ For both regions, ~~we observe~~ clear upward or downward trends in blocking frequency over the 30 years ~~no clear trend in the frequency of detected blocking events, however, the observed year-to-year~~ are not obvious. However, inter-annual variability is high~~(~~, see black squares in Fig. 6~~a~~,(a),(b). ~~Additionally the variability between the~~ Variability between different experiments is relative large, ~~although this spread shows no trend~~ this spread does, however, not show trends over time, ~~too (~~see gray boxes in Fig. 6~~a,b). Since the block numbers are given by integers, the boxes can be very large.~~ (a),(b)[5]. Considering the fraction of blocked time steps per year (green, Fig. 6~~a,b), the year-to-year~~ (a),(b)), the inter-annual variability is still obvious. However, the spread between the experiments is smaller. ~~No trend is observed~~There is no obvious trend, neither in the values of experiment E05 (corresponding to the lines in Fig. 6) nor in the spread ~~of~~ over all experiments. However, the spread is smaller in the Euro-Atlantic region (Fig.~~6b~~ 6(b)) compared to the larger ~~Northern Hemisphere~~ region (Fig.~~6a). With respect to the blocking lifetimes, we observe a very high year-to-year and intra-experimental variability for~~ 6(a)).

The mean duration of blocking events show a small inter-annual and inter-experimental variability compared to the maximum duration (~~blue, Fig.6c,d) in both regions. This maximum is of course~~ see red and blue crosses and bars in Fig. 6(c),(d)). Note, that the maximum is given by only one data point per year and experiment. ~~Therefore, the spread between the experiments is very large, but~~ The spread between experiments is thus very large in both regions, whereas smaller for the Euro-Atlantic region. ~~On the other hand, the mean duration remains relatively stable over the 30 year period for E05 as well as for all experiments considered (red, Fig. 6c,d), although the year-to-year variability is larger in the smaller domain.~~ Note, that the residence time of blocks in the smaller region also depends on the ~~travel~~ propagation speed of the blocking and a larger variability in the mean duration could be caused by a year-to-year variability of faster or slower ~~travel speeds.~~ propagation speeds.

[5] Note that block numbers can only take integer values.

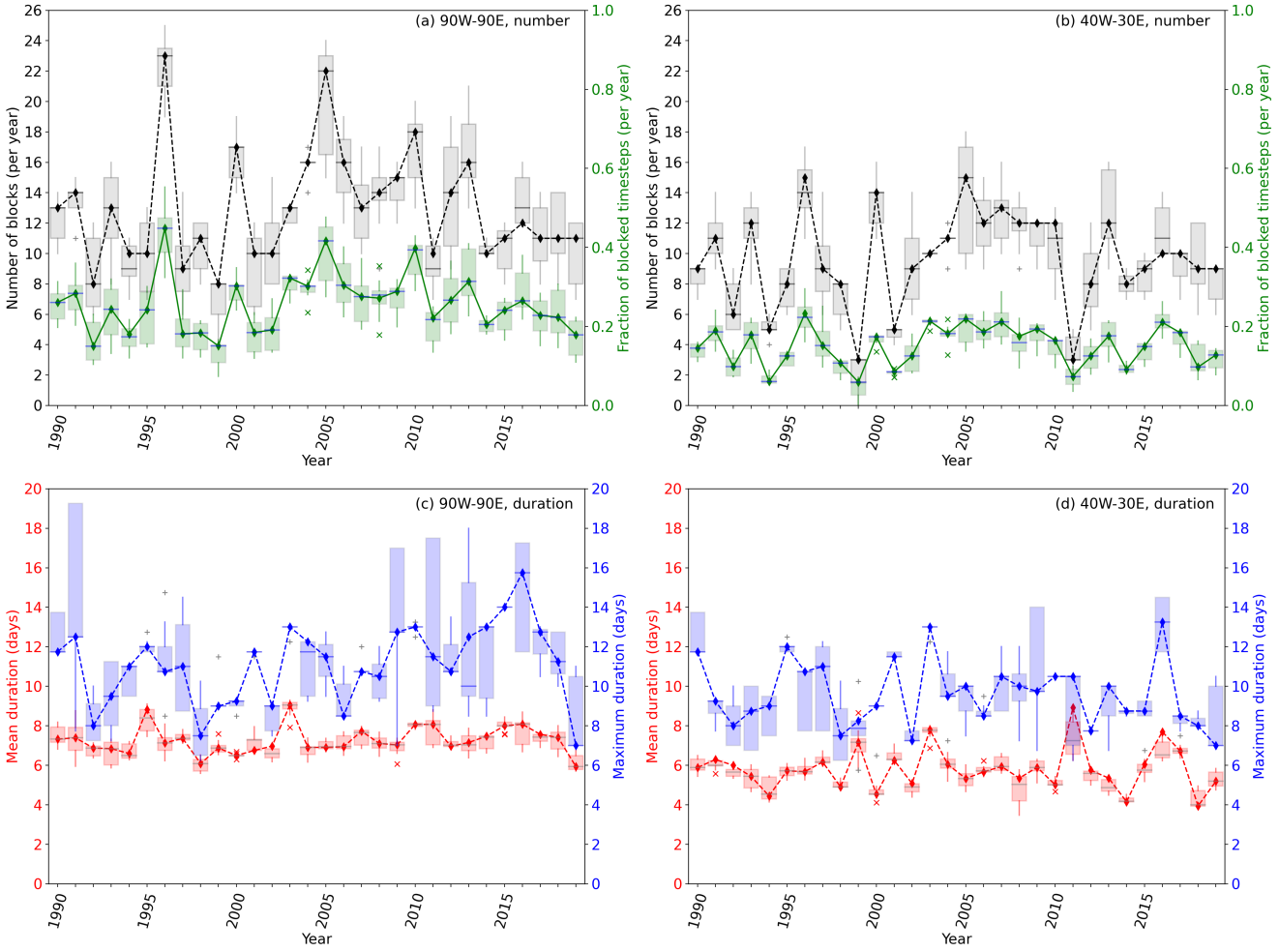

Figure 6. Temporal development of (a,b) blocking number (black) and fraction of annual blocked time steps (green); (c,d) mean (red) and maximum (blue) duration of a blocking event (a,c) for the whole domain ($90^\circ W$ to $90^\circ E$) and (b,d) for Euro-Atlantic region ($40^\circ W$ to $30^\circ E$). Boxes represent the ~~inner-quartile~~ interquartile range of the experiments described in Table 1 to test the uncertainty of the method for different distance criteria between two time steps. The whiskers are 1.5 times the ~~inner-quartile~~ interquartile range and single points in appropriate colors represent outliers. Note, that blocking numbers are given as integer. Experiment E05 is explicitly plotted in corresponding colors to the boxplots by symbols and lines. These lines are just plotted to ease the identification of E05.

4.2 Temporal development of blocking probabilities – ~~Two-states~~ Two-state blocking model

4.2.1 ~~Seasonal blocking probability~~

We investigate the inter-annual variability of blocking occurrence probability taking only two states into account: *blocking* and *no blocking*, both *Omega* and *High-over-low* blocks are for now considered as *blocking*. Starting with annual probabilities, we resolve the blocking occurrence seasonally and monthly in further steps.

~~Figure 7 shows the temporal evolution of blocking probability, i.e. the probability of a time step being part of a blocking event that lasted a minimum of 5 days, for the 30 year period separated by year and/or season. Probability is obtained with the logistic regression models using the season $\text{Seas} \in \{\text{DJF}, \text{MAM}, \text{JJA}, \text{SON}\}$ as a categorical term in the predictor~~

$$\text{logit}(p) \quad \sim \text{Year}\,,$$

$$\text{logit}(p) \quad \sim \text{Year} * \text{Seas}\,.$$

~~where the months December, January, February, etc.have been abbreviated by capital letters D, J, F, and so forth. In the following, we test parameter estimates being different from zero using the z-test~~

4.2.1 Annual blocking probability

We study annual blocking occurrence probability with ~~p-values encoded as~~ logistic regression as described in Sec. 3.5 using

$$0 < \text{logit}(^{***}p) < 0.001 < (^{**}) < 0.01 < (^{*}) < 0.5 \sim \text{Year}\,. \tag{22}$$

~~Blocking probability over time for the full *year* (black line, Eq.22) and for individual *seasons* (colored lines, Eq. 24). Shadings shows 95% confidence intervals. (a) 90° W to 90° E and (b) selected Euro-Atlantic region (40° W to 30° E).~~ The black lines in Fig. 7 ~~show the probabilities for the full year (Eq. 22) and the colored lines show the development of the blocking probability in the individual seasons using a model with interactions (Eq. 24). Within the study period, the annual blocking probability (black line) increases significantly(**) in the whole domain (Fig.7a~~shows the models expectation for the probability that a time step is part of a blocking event that lasted a minimum of five days (blocking occurrence probability) ~~and also significantly(*) in~~ for 90° W to 90° E (Fig. 7(a)) and the Euro-Atlantic region (~~Fig. 7b). However, these increases are rather small by two , and one percent points, respectively.~~ 40° W to 30° E, Fig. 7(b)). Shadings give 95% confidence intervals. We use a Wald-test (z-test) to test for a significant trend with years with p-values encoded as

$$0 < (^{***}) < 0.001 < (^{**}) < 0.01 < (^{*}) < 0.05 < ()\,. \tag{23}$$

We find an increase of two percentage points (**) for the large region and one percentage point (*) in the North-Atlantic region.

The average probability is about 25% blocked time steps in 90° W to 90° E and about 15% blocked time steps in 40° W to 30° E. ~~This~~ This is in accordance with the fraction of blocked time steps per year plotted in Fig.~~6a,b~~ 6 (a),(b).

~~Using season as interaction effect in the regression~~

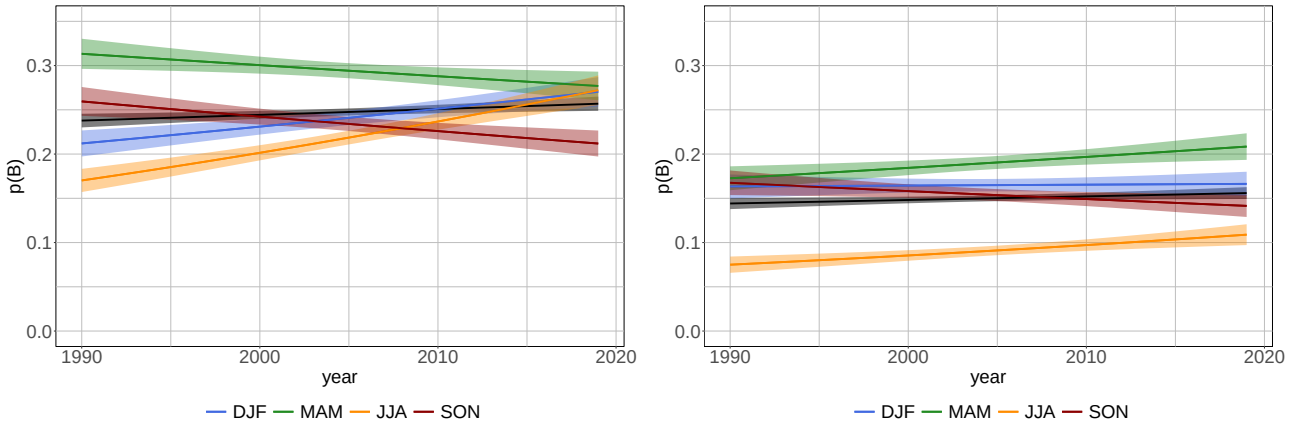

(a) 90° W to 90° E (b) 40° W to 30° E

Figure 7. Blocking probability over time for the full *year* (black line, Eq. (22)) and for individual *seasons* (colored lines, Eq. (24)). Shadings shows 95% confidence intervals. (a) 90° W to 90° E and (b) selected Euro-Atlantic region (40° W to 30° E).

4.2.2 Seasonal blocking probability

The coloured lines in Fig. 7 show analogously the expectation resolved by season obtained with a model with interactions (Eq. 24) ~~reveals that this increase~~

$$\text{logit}(p) \sim \text{Year} * \text{Seas} \tag{24}$$

with $\text{Seas} \in \{\text{DJF}, \text{MAM}, \text{JJA}, \text{SON}\}$ being a categorical term in the predictor. The months December, January, February, etc. have been abbreviated by capital letters D, J, F, and so forth. The seasonal resolution now allows to assign the increase for the region 90° W to 90° E over the 30 years ~~stems~~ to a large extend ~~from~~ to a significant increase of occurrence probability of blocked time steps in ~~the summer months~~ summer (JJA)(***) ~~from $p \approx 0.17$ to $p \approx 0.27$ in 90° W to 90° E (~~and winter (DJF)(***). During spring (MAM)(*) and autumn (SON)(***) occurrence probability is decreasing (see Fig. 7 ~~a~~(a)).

In the Euro-Atlantic region, the occurrence probability increase is weaker in Summer (JJA). ~~Furthermore, in the larger domain the probability of blocked time steps in winter (DJF)~~(***) ~~increases significantly, too, while the probability decreases in spring (MAM)(*)and autumn (SON)(***~~and not significant in Winter (DJF)()~~(Fig. 7a). In contrast to the decreasing probability observed for the spring season in the larger region (Fig. 7a, green line), we observe a significant increase in~~ . However, we observe now an increase in probability also in spring (MAM)(***)~~in the Euro-Atlantic sector (Fig. 7b, green line). The probability of blocking increases significantly in summer (JJA)(***), too, although summer yields the lowest probability of all seasons in the Euro-Atlantic region (Fig. 7b, yellow line). Moreover, 7 out of the 11 experiments show this significant increases in spring and summer. Autumn and winter show no significant trends in the Euro-Atlantic sector.~~ ; in autumn (SON)() the slight

decrease is not significant. The difference between the two regions suggest that the occurrence behavior of blocking is not the same across the larger region $90° W$ to $90° E$.

4.2.3 Monthly blocking probability in the Euro-Atlantic region

~~With a~~ We now break down trends in occurrence probability in the Euro-Atlantic sector to a monthly resolution using a categorical term for the month $\mathrm{Mon} \in \{1, 2, 3, \ldots, 12\}$ in the predictor, interacting with Year

$$\mathrm{logit}(p) \sim \mathrm{Year} * \mathrm{Mon} \text{ ,.} \tag{25}$$

~~we have more temporal detail and can pinpoint the drivers of the observed~~ Figure 8 shows monthly resolved trends in blocking

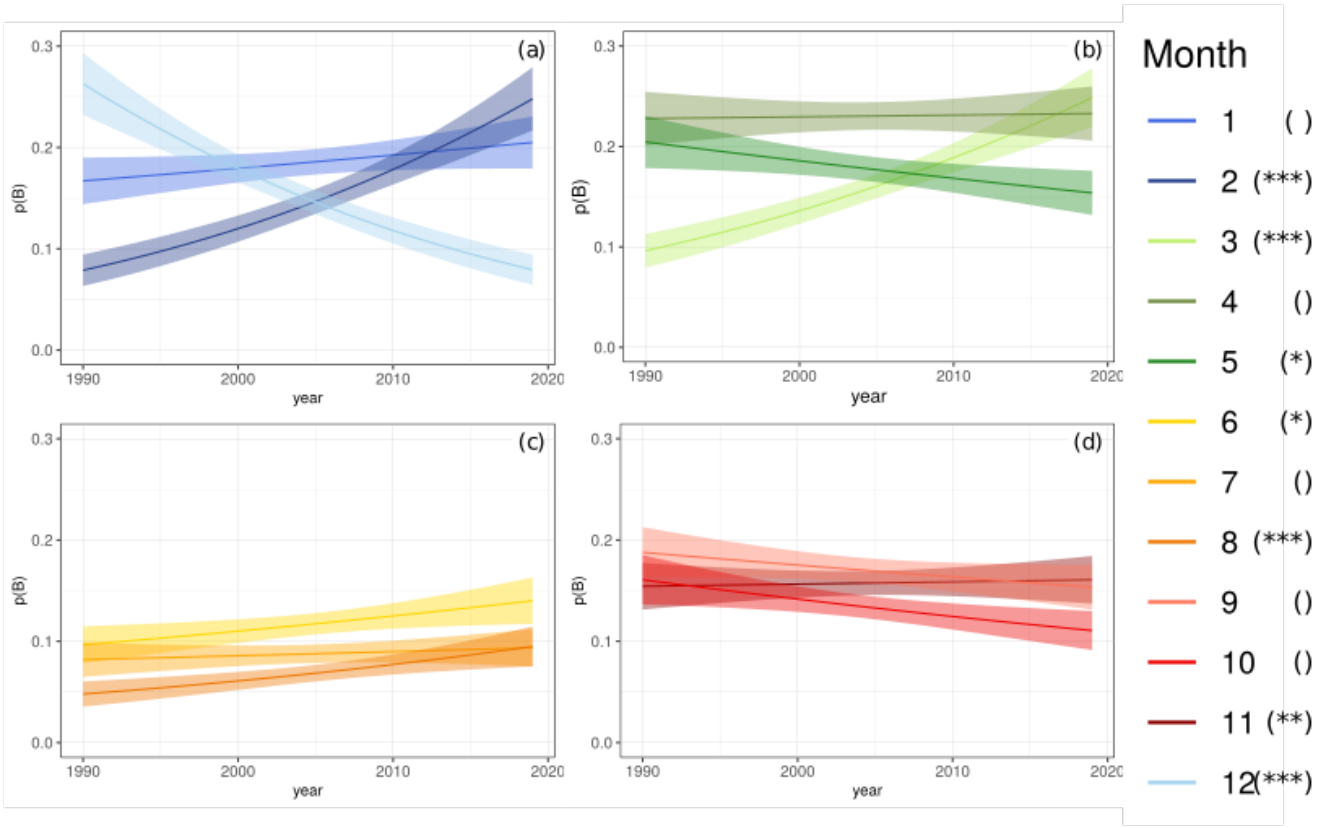

Figure 8. Blocking probability over time for individual *month* (Eq. 25). Shadings show 95% confidence intervals. (a) winter (DJF) (b) spring (MAM) (c) summer (JJA) and (d) autumn (SON) in the Euro-Atlantic region ($40° W - 30° E$). Significance is encoded as $0 <$ (***) $< 0.001 <$ (**) $< 0.01 <$ (*) $< 0.05 <$ ().

~~probability in~~ occurrence probability for the Euro-Atlantic ~~sector down to specific months (see~~ region. Panel (a) in Fig. 8 ~~).~~

Blocking probability over time for individual month (Eq. 25). Shadings show 95 % confidence intervals. (a) winter (DJF) (b) spring (MAM) (c) summer (JJA) and (d) autumn (SON) in the Euro-Atlantic region ($40° W - 30° E$).

All summer months, especially June and August, show a slight, but steady increase of blocking probability (see Fig. 8c, not significant) and contribute likewise to the observed general increase in summer (suggests that a strong decrease in December (***) compensated by a strong increase in February (***) and a weak increase in January () result in the approximately constant occurrence probability shown in Fig. 7right, yellow-orange line(b). Similarly, the general decrease of blocking observed in autumn (SON) is mirrored in all months, too, especially in September and October (in Fig. 8d,(*)). On the other hand, the the winter and spring seasons show more disagreements. For example, we observe an increase in Spring (MAM) on a seasonal basis. This increase can mainly be attributed to a strong significant increase of blocked time steps in (b) we see that the strong increase in blocking probability in March (***) from about 10% blocked time steps in 1990 to about 25% in 2019. While April is relatively stable over the whole period, we observe a significant decrease of blocked time steps for May (**) . However, this decrease is smaller in magnitude from about 20% to about 15% than the increase in March.The winter months (DJF) show no clear trend over the 30-year period on a seasonal basis is partly offset by a weaker decrease in May (*) while April is approximately constant. This is consistent with the increase visible for spring in Fig. 7(b). The summer month June (*) and August (***) exhibit an increase in blocking occurrence probability, the change in July is not significant (Fig. 7a, blue line). But the single months show a different behaviour (8(c)). This consistent increase adds up to the significant increase observed for summer in Fig. 7(b). In autumn, we see a decrease in November (**) and non-significant changes for September and October (Fig. 8a): While blocked time steps in December(***)decrease significantly, the probability for blocked time steps in February increases strongly (***)for the same period. (d)). This is reflected in the slight and not significant increase seen for autumn in Fig. 7(b). Moreover, all experiments with different distance criteria agree on the significant decrease in December and the significant increases in February, March and August. A significant decrease in October is only observed for the 6 experiments with the strictest distance criteria

The consistency between seasonally and monthly resolved results give confidence in the analysis. Furthermore, it seems worth looking at both resolutions as strong monthly resolved signals can average out when aggregated to the season as in winter or weak but consistent monthly signals can add to a stronger seasonal signal as in summer. The monthly resolution now allows to postulate that in the Euro-Atlantic region there are signs for blocking occurrence probability increases at the beginning of the year (JFM) and decreases towards the end of the year (SOND); inter-annual variation in between is comparably small.

4.3 Temporal development of blocking probabilities – Three-states Three-state blocking model

In the following, we We now additionally distinguish between the two blocking types *High-over-Low* and *Omega*blocks using the three-states , considering occurrence probabilities for three states in a multinomial logistic model.

4.3.1 The annual Annual cycle of blocking probability

Taking a look at the annual cycle of blocking probability reveals that the colder months from September to March are characterized by relatively high, but stable blocking probabilities of about 22% ($\approx 15\%$) in $90° W$ to $90° E$ ($40° W$ to $30° E$) with a

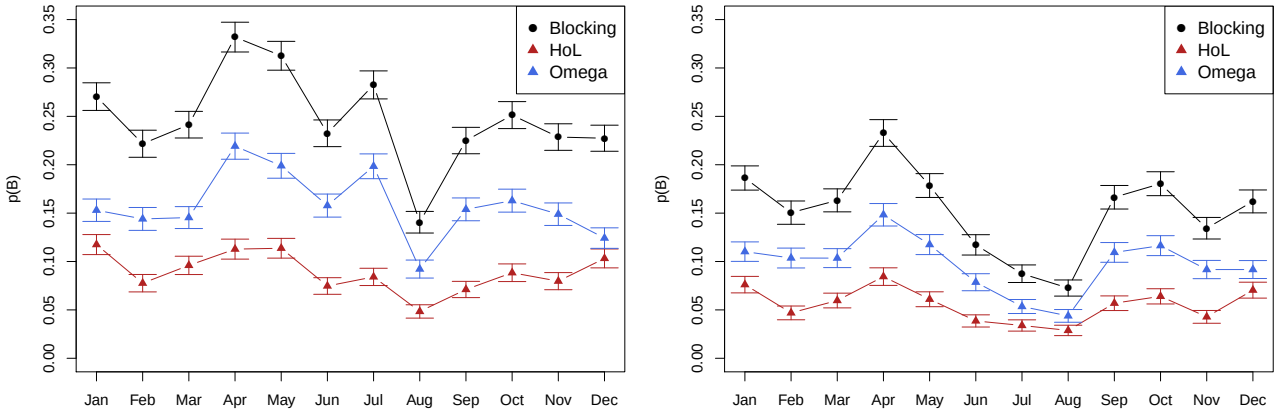

(a) 90° W to 90° E

(b) 40° W to 30° E

Figure 9. Blocking probability estimated for individual months for blocking in general, as well as separately for *High-over-Low* and *Omega*. (a) whole domain (90° W to 90° E) and (b) Euro-Atlantic subsection (40° W to 30° E). Whiskers shows 95% confidence intervals assuming Gaussian asymptotic for estimating binomial probabilities.

smaller peak in January (see Fig. 9). The main peak in both regions occurs in April. While the larger region (90° W to 90° E) shows a broader peak with high values also in May and a secondary peak in July, in the Euro-Atlantic region the blocking probability only peaks in April and shows a broader minimum in June to August. In the larger region, the lowest blocking probability occurs in August, too, but June and July have higher probabilities. In general, about 2/3 of the blocked time steps can be classified as *Omega* blocks and about 1/3 as *High-over-Low* blocks. Only in December and January, this classification rather changes to about 1/2 (both regions, red/blue triangles in Fig. 9). ~~It should be noted~~ Note that a blocking does not have to occur in every month of every year (see Supplementary Material Fig. S.6 and Fig. S.7). ~~Further differences can be seen for the two types of blocking. For~~ The occurrence frequency of *Omega* blocks ~~, greater fluctuations can be seen within the individual years~~ shows a larger intra-annual fluctuation (see Supplementary Material Fig. S.6 and Fig. S.7 for more details). ~~At this point it should also be pointed out that it~~ It is possible that only a few time steps of a blocking lie in one month while the other time steps are in an adjacent month.

4.3.2 Seasonal ~~and monthly~~ blocking ~~probability~~ probabilities in the Euro-Atlantic sector

~~The three-state blocking model~~ Having now three states with distinct *High-over-Low* and *Omega* blocks~~can be described in a similar manner as the two-state Markov model but using~~ , we use multinomial logistic regression (Sec.3.5) with reference

$Pr\{Y_t = nB|Y_{t-1}\}$. The ~~models used here are~~ basic model is given by

$$\ln\left(\frac{Pr\{Y_t = HoL\}}{Pr\{Y_t = nB\}}\right) \sim \text{Year} * , \qquad \ln\left(\frac{Pr\{Y_t = \Omega\}}{Pr\{Y_t = nB\}}\right) \sim \text{Year} * , \ln\frac{Pr\{Y_t = HoL\}}{Pr\{Y_t = nB\}} \sim * , \ln\frac{Pr\{Y_t = \Omega\}}{Pr\{Y_t = nB\}} \sim * . \tag{26}$$

~~As described in Sec. 3.5, for both cases, the seasonal and the monthly case, we need two equations,~~ using two equations: one for $Pr\{Y_t = HoL\}$ and one for $Pr\{Y_t = \Omega\}$. This can be straightforwardly extended to seasonally resolved trends by

$$\ln\left(\frac{Pr\{Y_t = HoL\}}{Pr\{Y_t = nB\}}\right) \sim \text{Year} * \text{Seas}, \qquad \ln\left(\frac{Pr\{Y_t = \Omega\}}{Pr\{Y_t = nB\}}\right) \sim \text{Year} * \text{Seas}, \tag{27}$$

To avoid problems with significance testing due to the Hauk-Donner effect (Yee, 2015, Chap. 2.3.6.2), we avoid the Wald-test in favor of a likelihood-ratio test. This implies that we test the null hypothesis of constant probabilities against the alternative with probabilities depending on the covariate Year. Consequently, we cannot infer significant trends in occurrence probability *individually* for *High-over-Low* or *Omega*.

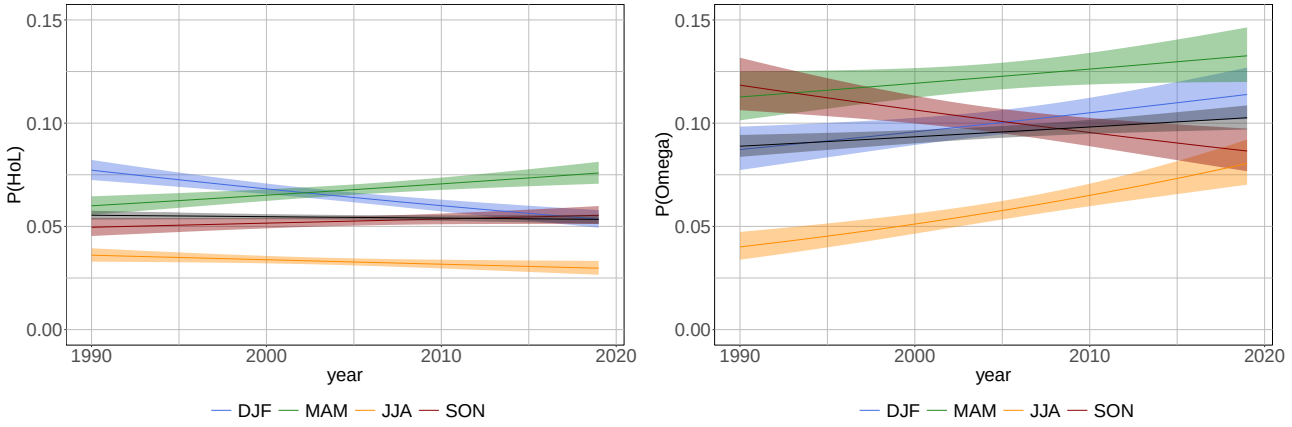

(a) High-over-Low blocking, 40° W to 30° E

(b) Omega blocking, 40° W to 30° E

Figure 10. ~~Temporal development~~ Blocking probability over time for the full *year* (black line, Eq. 26) and for individual ~~seasons~~ *seasons* (colored lines, Eq. ~~-~~27) for the ~~blocking probabilities for the~~ Euro-Atlantic ~~region~~ (40° W − 30° E) region for (a) *High-over-Low* and (b) *Omega* blocking. Shadings shows 95% confidence intervals.

Figure 10 shows the expectation of the multinomial model (Eq. 27) for the temporal evolution of the probabilities of the two blocking types for annual occurrence probabilities (black line) and broken down to ~~the seasons . The probability of~~ seasons (coloured lines). Annual occurrence probabilities are constant for *High-over-Low* ~~blocks in the Euro-Atlantic region shows a decrease/slight decrease in winter(DJF) /summer (JJA,(**)) and an increase /slight increase in spring (MAM,(*))/autumn (SON, (~~and slightly increase (*)~~) over the 30-year period (see ~~)~~ for *Omega*. In winter, we observe a significant (***) decrease

of *High-over-low* (Fig. 10(a)) which is offset by an increase in *Omega* (Fig. 10(b))[6], leading to almost constant overall blocking in that season (Fig. ~~10a)~~[7]~~. At the same time, the probability for~~ 7(b)). The overall increase in blocking probability in spring, seen earlier in Fig. 7(b), can now be attributed to a significant (*) increase in both, *High-over-low* and *Omega* ~~blocks increases strongly in the summer months (***)and also pronounced in winter(**) and spring (~~blocking, see Fig. 10~~b). Only the *Omega* blocks in autumn (SON,(**)) decrease over the 30 years~~[7]. ~~Interestingly, the blocked summer *High-over-Low*s start with the same probability as the~~ In summer (***), a strong increase in *Omega* ~~blocks in the 1990s. However, while the probability increases strongly for *Omega* blocks, it shows only a very slight increase for~~ occurrence probability is partly offset by a decrease in *High-over-Low* ~~s. Hence, the observed, general~~ leading to a significant increase in summer blocking ~~probability (~~occurrence in Fig. 7(b)[7]. The weak autumn decrease in total blocking occurrence in Fig. 7(b) can now be attributed to ~~an increase~~ a strong (**) decrease in *Omega* ~~block patterns. This increase occurs in all three summer months, but stronger in June and August (see~~ blocks which is only partly offset by an increase in *High-over-Low* occurrence (Fig. ~~8c). Blocking probability over time for individual month (Eq. 28) for *High-over-Low* (solid) and *Omega* (dashed) blocking. Shadings show 95% confidence intervals. (a) winter (DJF) (b) spring (MAM) (c) summer (JJA) and (d) autumn (SON) in the Euro-Atlantic region ($40° W - 30° E$).~~ 10)[8].

~~A refinement based on monthly resolution is shown in Fig. 11. In the winter season, we observe an increase of~~

4.3.3 Monthly blocking probability in the Euro-Atlantic sector

We now estimate monthly resolved trends in blocking occurrence probabilities for the three-state model in Eq. (28).

$$\ln\left(\frac{Pr\{Y_t = HoL\}}{Pr\{Y_t = nB\}}\right) \sim \text{Year} * \text{Mon}, \qquad \ln\left(\frac{Pr\{Y_t = \Omega\}}{Pr\{Y_t = nB\}}\right) \sim \text{Year} * \text{Mon}\,. \tag{28}$$

Figure 11 shows the expected occurrence probabilities for ~~*Omega*~~*High-over-Low* ~~blocks in February and January and a decrease in December (Fig. 11a,~~ (solid lines) and *Omega* (dashed lines) ~~. The~~ blocking resolved by month. Significance from a likelihood-ratio test is again given in the legend of the plot. The probabilities of *Omega* and *High-over-Low* ~~blocking~~ agree on the decrease in December and ~~January and only slightly~~ increase in February~~(see Fig.11a)December and January are significant (***) for both blocking types, February is only significant for~~ , consistent with Fig. 8(a); in both cases the trend for ~~*High-over-Low*~~*Omega* ~~s (**). In spring, the probabilities for~~ blocks is stronger. In January, the increase in *Omega* is partly offset by the decrease in *High-over-Low*~~blocking remain more or less constant, with only~~ , leading to a slight increase in ~~March.~~total blocking for this month (Fig. 8(a)). Figure 11(b) shows that *Omega* and *High-over-Low* occurrence probabilities increase

[6] 8 (*Omega*) and 11 (*High-over-Low*) out of 11 experiments agree on the trend in DJF and confidence intervals are not compatible with a constant occurrence/transition probability.

[7] ~~All 11 experiments agree on the decrease of *High-over-Low* probabilities in DJF and 9 out of 11 experiment show the significant increase in SON.~~

[7] ~~For the *Omega* blocks 10 out of 11 (8 out of 11) experiments agree on the significant increase in JJA (DJF). All experiment agree on a decrease in SON, but only 5 of them are significant.~~

[7] 10 out of 11 experiments agree on the increasing trend of the *Omega* blocks in JJA and confidence intervals are not compatible with a constant occurrence/transition probability.

[8] 9 (*High-over-Low*) and 5 (*Omega*) out of 11 experiments agree in the trend in SON and confidence intervals are not compatible with a constant occurrence/transition probability.

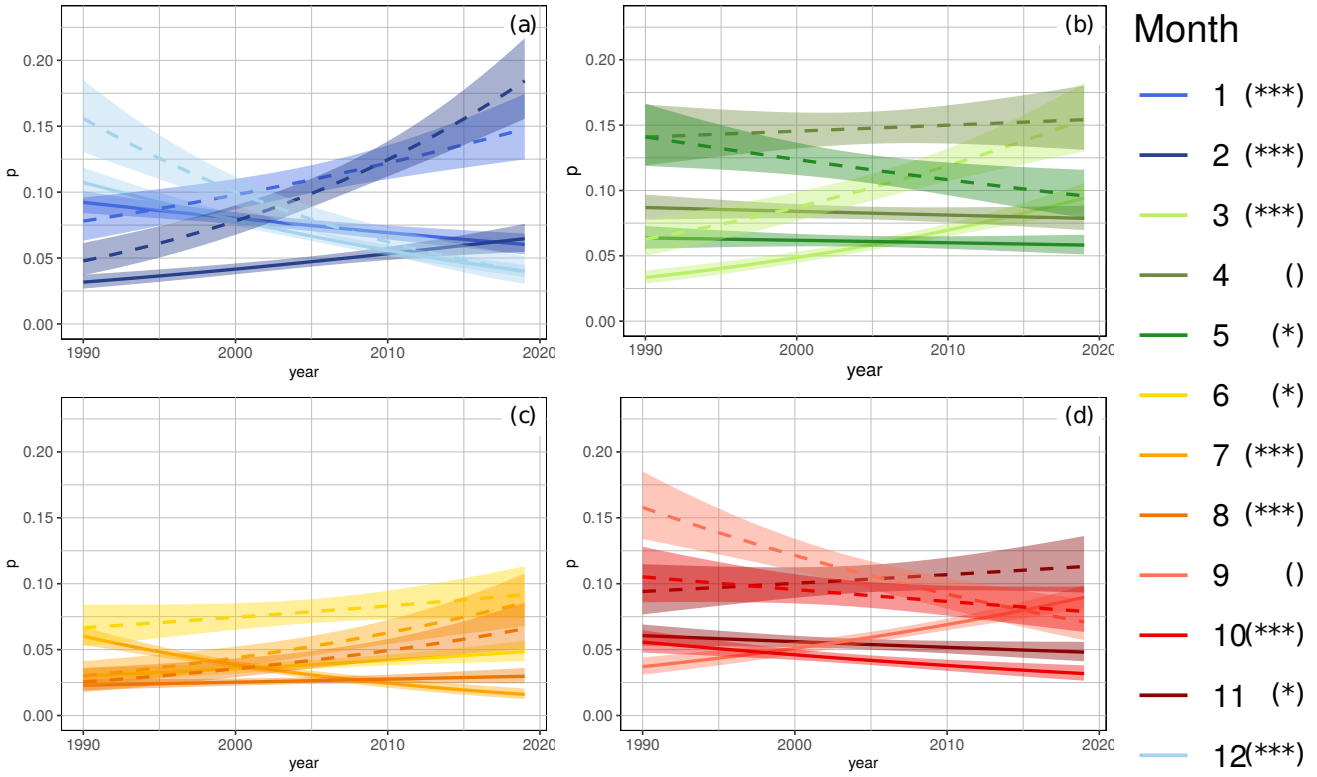

Figure 11. Blocking probability over time for individual *month* (Eq. 28) for *High-over-Low* (solid) and *Omega* (dashed) blocking. Shadings show 95% confidence intervals. (a) winter (DJF) (b) spring (MAM) (c) summer (JJA) and (d) autumn (SON) in the Euro-Atlantic region ($40° W - 30° E$). Significance is encoded as $0 < (***) < 0.001 < (**) < 0.01 < (*) < 0.05 < ()$.

simultaneously in March and decrease simultaneously in May, being consistent with the trends of total blocking occurrence in that month (Fig. 8(b)). April shows weakly increasing (*Omega*~~blocks therefore play agreater role in the development of these frequencies here as well. The highest change is in March(***) and a decrease in May~~) and decreasing (*High-over-Low*) trends averaging out to almost constant total blocking (~~***) (see Fig.11b)~~Fig.~~In the summer months the change is not as pronounced as in the other seasons and is again mainly dominated by *Omega* blocks (see Fig. 11c,not significant) . In autumn there is no significant trend in the blocking probability of the two-state model (see Fig.7b). An analysis of the individual months shows a slight increase in the probabilities in November for *Omega* blocks (not significant) and a decrease for *High-over-Low*s(~~ 8(b)). Panel (c) of Figure 11 shows a weak increase in June (*) and August (***) occurrence probability for both blocking types, consistent with the weak increase of total blocking shown in Fig. 8(c). In July (***)~~. The other two months, however, show a decrease for~~ , *High-over-Low* is decreasing while *Omega* ~~blocks. For~~ is increasing resulting in very weakly increasing total

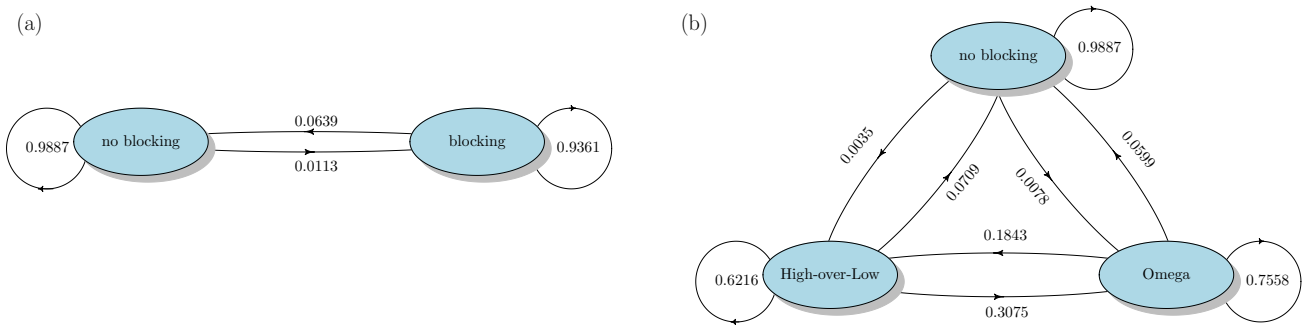

Figure 12. Graph representation of ~~transition probabilities of~~ the transition matrix estimated for a Markov process (a) with two states (Eq. 17) and (b) with three states (Eq. 18) in the Euro-Atlantic region ($40° W - 30° E$). Standard errors of the estimates are given in Tables. 2 and 3.

blocking probability (Fig. 8(c)). In October, both blocking types decrease (***) consistently as well as the overall blocking probability. In September () *Omega* decreases while *High-over-Low* ~~blocks a slight increase is shown for September and a decrease in October. All in all, this balances itself out.~~increases and vice versa in November (*); both leading to almost constant total blocking occurrence probability in the two months, see Fig. 8(d).

4.4 Transition probabilities

We conceive the dynamics between different blocking and no-blocking states as a stochastic process with Markov properties (see ~~Section~~Sec. 3.6)~~and~~ . We can thus give transition probabilities for the two- and ~~three-states model with stationary and non-stationary assumptions in the following.~~

4.4.1 ~~Transition probabilities of two- and three-state models~~

~~Assuming~~ three-state model in the Euro-Atlantic region. We start with assuming a homogeneous Markov process and give stationary transition probabilities~~, we can estimate transition matrices for the two- and three-state models.~~. In a second step, we allow transition probabilities to vary with years. Analogously to the model presented in Sec. 4.3.2, we break the trends in years down to the four seasons.

4.4.1 Transition probabilities of two- and of three-state models

Within the framework of homogeneous Markov processes, we estimate stationary transition probabilities. Figure 12 ~~shows the transition probabilities of~~ visualize the transition matrices for the two-state ~~Markov model with~~ model (*no blocking* and *blocking*~~(Fig. 12)~~ in panel (a) and the three-state ~~Markov model with the states~~ model (*no blocking*, *High-over-Low* and *Omega*~~*block(Fig. 12* block~~) in panel (b). ~~We call the probability to remain in one state *stability* or *persistence* and the transition from *no blocking* to a *blocking* (*High-over-Low* or *Omega*)~~ The estimate for the transition probability from *no blocking* to *blocking* is $p_{nB,B} = 0.0113$, denoting that in about 1% of all time steps (6 hours resolution) we observe an *onset* ~~which~~

~~indicates the formation of a blocking; the opposite direction is called *offset* which can also be seen as a decay. In this work we will stick with the terms~~ of blocking. Being in a blocked state, we estimate the ~~*onset*~~*persistence* ~~and *offset* as we focus on the model view, in which there is only the state "on" or "off". From a meteorological point of view, the use of the word "decay" describes the transformation from~~ to remain in this state as $p_{B,B} = 0.9361$ and the *decay* to a non-blocked state as $p_{B,nB} = 0.0639$. Thus, being in a blocked state~~to an unblocked state with the right words, as it is a process. For both models, persistence (~~, the probability to remain ~~in one state) of either state is higher than transition probabilities to other states; particularly high is the persistence of the no-blocking state. The latter is due to the fact that there are considerably more time steps without blocking than blocked states. But if blocking occurs, the~~ (*persistence*) there is about 94% and the probability that this blocking *decays* is about 6%. Being in the *no-blocking* state, we find a probability to remain ~~in this condition is high, too~~there of $p_{nB,nB} = 0.9887$.

~~For the three-states model, the onset probability for~~ Considering the three-state model, we can now break down the total blocking *onset* probability into the *onset* of *High-over-Low* ($p_{nB,HoL} = 0.0035$) and the *onset* of *Omega* ($p_{nB,\Omega} = 0.0078$). Thus in about two of three blocking *onsets*, we see an *Omega* blocking ~~is higher than that for~~ rather than a *High-over-Low*~~blocking. Both values are small compared to the persistence defined above. This is consistent with the fact that onsets are less frequent. With this model , we obtain that~~ [9]. This does not hold for the *offset* as in the three-state model offset probability is conditioned on *Omega* ~~blocking is~~ or *High-over-Low*. Furthermore, we see two indications for *Omega* blocks being more stable than *High-over-Low*~~blocking, i.e. $Pr\{Y_t = \Omega \mid Y_{t-1} = \Omega\} > Pr\{Y_t = HoL \mid Y_{t-1} = HoL\}$. Moreover, a *High-over-Low* block evolves more likely into an *Omega* block than vice versa. This means that another low-pressure system disturbs the~~ s: i) the ~~*High-over-Low*~~*persistence* ~~block and the structure changes to an~~ of *Omega* blocking ~~. This occurs more often than that a low pressure system leaves the *Omega* block and thus turns the system into a~~ is with $p_{\Omega,\Omega} = 0.7558$ larger than the persistence of *High-over-Low* ~~pattern. The offset (or decay)of an *Omega* block to the unblocked state is also less likely than the decay of a~~ ($p_{HoL,HoL} = 0.6216$), and ii) the *transition* from *High-over-Low* ~~block, i. e. $Pr\{Y_t = nB \mid Y_{t-1} = \Omega\} > Pr\{nB \mid Y_{t-1} = HoL\}$.~~ to *Omega* is with $p_{HoL,\Omega} = 0.3075$ larger than the reverse transition with $p_{\Omega,HoL} = 0.1843$. Probability estimates and standard errors are given in Tables 2 and 3.

Table 2. Probability estimates ± standard errors for the two-state model. Probabilities give the transition to the state given in the column conditioned on the state given in the row.

	nB	B
nB	0.09887 ± 0.0052	0.0113 ± 0.0006
B	0.0639 ± 0.0031	0.9361 ± 0.0119

4.4.2 Trends of transition probabilities of two- and of three-state models

[9] Note that for blocking *onset*, both probabilities ($p_{nB,HoL}$ and $p_{nB,\Omega}$) are conditioned on the *no-blocking* state and thus $p_{nB,HoL} + p_{nB,\Omega} = p_{nB,B} = 0.0113$ sum up to the total *onset* probability.

Table 3. Probability estimates ± standard errors for the three-state model. Probabilities give the transition to the state given in the column conditioned on the state given in the row.

	nB	HoL	Ω
nB	0.9887 ± 0.0052	0.0035 ± 0.0003	0.0078 ± 0.0005
HoL	0.0701 ± 0.0055	0.6216 ± 0.0161	0.3075 ± 0.1136
Ω	0.0599 ± 0.0038	0.1843 ± 0.0066	0.7558 ± 0.0134

~~Of particular interest is a potential change in transition probabilities during the study period 1990 to 2019. For this purpose, we~~ We describe the change in transition probabilities with time (years) using logistic and multinomial regression~~with year (and season) as interacting terms in the predictor.~~ , on the annual time scale and broken down into seasons.

For the two-state Markov model (Eq. (19)) no significant changes ~~neither with year as given in Eq. 19 (~~can be identified, neither for the full-annual probabilities, nor broken down into seasons, see Supplementary Material ~~Fig.~~Figs. S.8 ~~) nor with interacting terms for year and season~~

$$\text{logit}(Pr\{Y_t = B \mid Y_{t-1}\}) \quad \sim Y_{t-1} * \text{Year} * \text{Seas},$$

~~(see Supplementary Material Fig.~~ and S.9~~) are identified. Breaking this down to a~~ .

Changes in transition probabilities for the three-state Markov model ~~we get the following equation for yearly changes~~ with annual occurrence probabilities are described by

$$\ln\left(\frac{Pr\{Y_t = HoL\} \mid Pr\{Y_{t-1}\}}{Pr\{Y_t = nB \mid Y_{t-1}\}}\right) \sim Y_{t-1} * \text{Year}, \qquad \ln\left(\frac{Pr\{Y_t = \Omega\} \mid Pr\{Y_{t-1}\}}{Pr\{Y_t = nB \mid Y_{t-1}\}}\right) \sim Y_{t-1} * \text{Year}\,. \tag{29}$$

~~and Eq. 20 and 21 (see also Sec. 3.6) for the trends with interacting terms for year and season.~~

Figure 13 shows the temporally varying transition probabilities for the three-state model as a function of the year. Rows and columns are arranged analogously to the transition matrix (Eq. ~~18). The~~ (18), Table 3), shadings give 95% confidence intervals.

~~Transition probabilities analogous to the matrix of a three-state Markov process (Eq. 18) as a function of years (Eq. 29) in the Euro-Atlantic region ($40° W - 30° E$). (a) $p_{nB|nB}$, (b) $p_{HoL|nB}$ (c) $p_{\Omega|nB}$, (d) $p_{nB|HoL}$, (e) $p_{HoL|HoL}$ (f) $p_{\Omega|HoL}$, (g) $p_{nB|\Omega}$, (h) $p_{HoL|\Omega}$ and (i) $p_{\Omega|\Omega}$. Shadings show 95 % confidence intervals.~~

~~Similar to the tendency we see in the two-state model , the probability for remaining in an unblocked state~~ Analogously to Sec. 4.3.2, we use the likelihood-ratio test to infer whether inclusion of the trend in years results in a significantly better model than the homogeneous Markov process. With a p-value < 0.05 we find significance on the 5% level. Besides the first row, confidence intervals are larger than the signal itself and we refrain from detailed inferences on the trends for transitions from the two blocking states *High-over-Low* and *Omega*. However, we can see a positive trend for the transition from *no-blocking* to *Omega* (Fig. 13~~a)slightly decreases and the onset probability of~~ (c)) and a consistent decline of the persistence of

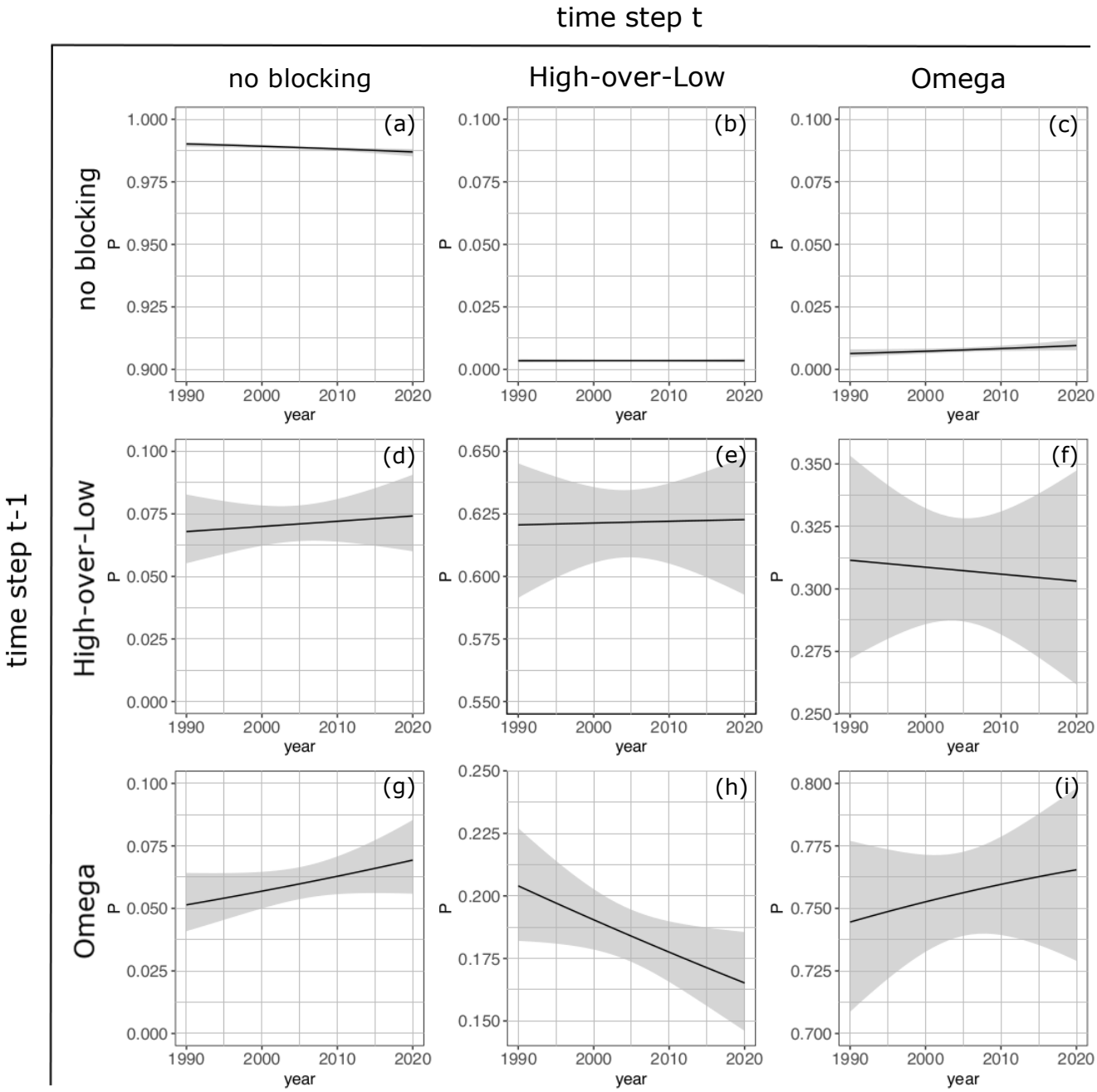

Figure 13. Transition probabilities analogous to the matrix of a three-state Markov process (Eq. 18) as a function of *years* (Eq. 29) in the Euro-Atlantic region ($40° W - 30° E$). (a) $p_{nB|nB}$, (b) $p_{HoL|nB}$ (c) $p_{\Omega|nB}$, (d) $p_{nB|HoL}$, (e) $p_{HoL|HoL}$ (f) $p_{\Omega|HoL}$, (g) $p_{nB|\Omega}$, (h) $p_{HoL|\Omega}$ and (i) $p_{\Omega|\Omega}$. Shadings show 95 % confidence intervals.

~~*Omega*~~*no-blocking* ~~blocks~~ states (Fig. 13~~c)slightly increases. For the three-state Markov model, these trends are significant[10]. Note also the decrease of transition probability from~~ (a)), while the transition from ~~*Omega*~~*no blocking* to *High-over-Low* $p_{HoL|\Omega}$ is approximately constant (Fig. 13~~h~~[10]~~)which is compensated by an increase in persistence of *Omega* $p_{\Omega|\Omega}$~~ (b)). This is in line with i) the slight increase of overall blocking probability (Fig. ~~13i)and an increase of offset probability from~~ 7(b), black line) and ii) the increase of *Omega* blocking $p_{nB|\Omega}$ (Fig. ~~13g) (all three not significant). We can thus refine the impression from the two-state model:~~ 10(b), black line). It further indicates that *Omega* blocking are more ~~frequent and those are predominantly *Omega*, which become more stable and do less likely evolve into *High-over-Low*s.~~ favoured for a blocking *onset* towards the end of our study period.

We now use the model given in Eqs. (20) and (21) to break the previous results down into seasons. Analogously to Fig. 13, Figure 14 shows trends in transition probabilities with lines colored according to the season.

~~Breaking this down into seasons by adding another interaction effect (Eq. 20 and Eq. 21), we obtain~~ Inclusion of the trend in years broken down to seasons is – according to the likelihood-ratio test – a significant improvement over a homogeneous Markov process for summer (JJA, (***)), winter (DJF, (*)) and spring (MAM, (*)); for autumn (SON), improvement is not significant on the 5% level. Panel (c) in Fig. 14 ~~. The largest temporal changes can again be observed in the summer months. The first row shows an increase in the onset probability for~~ now suggests that the previously observed increase in blocking *onset* to *Omega* (Fig.~~14c)blocks in summerwhile the probability of remaining in a no blocking state (Fig.14a)decreases (both significant,*). The last row shows that *Omega* blocks (Fig. 14i) become~~ 13(c)) is strongest in summer, weaker in spring and winter and even reversed in autumn. This is consistent with the negative trend in the probability to remain in a *no-blocking* state being strongest in summer (panel (a)). For most other cases, the confidence intervals are so large, that they are also consistent with constant probabilities. Detailed interpretation is thus to be taken with care. Having that said, panel (e) suggests that *High-over-Low* becomes slightly more stable in ~~summer towards the end of the study period and becomes less likely to evolve into a *High-over-Low* (Fig.14h)(both not significant). Changes~~ spring and autumn and less stable in summer and winter; stability for *Omega* is even less clearer to determine from panel (i), however a slight increase in winter and decrease in spring can be observed (in both cases confidence intervals are compatible with a constant transition probability). Further interesting aspects are changes in transition probabilities ~~for~~ from *Omega* to *High-over-Low* ~~blocks are in the second row of Fig.14: A decrease in persistence in summer and an increase in stability in the other seasons (Fig.14e)(all not significant). The transition probabilities towards~~ and vice versa. These are difficult to infer based on the data set used here (large confidence intervals). However, there seems to appear a slight increase in transitions from *High-over-Low* to *Omega* ~~blocks (Fig.14f) increase strongly in summer and slightly~~ in winter and summer; the opposite transitions in winter and ~~decrease in the transition seasons (all not significant). Although not significant, this confirms again the previously gained impressions: *Omega* blocks become more frequent and stable in summer and the transition probability of~~ summer decrease. Furthermore, *High-over-Low* to *Omega* ~~decreases in summer. The persistence of *High-over-Low*s~~ increases over the years in the transition seasons and become

[10] ~~All experiments agree on the decrease in persistence of the unblocked state (8 out of 11 show a significant decrease) and all agree on the increase of the onset probability of the *Omega* blocks (6 out of 11 significantly)~~

[10] ~~6 out of 11 experiments show a significant decrease of the transition probability from *Omega* to *High-over-Low*, all agree on the decrease however.~~

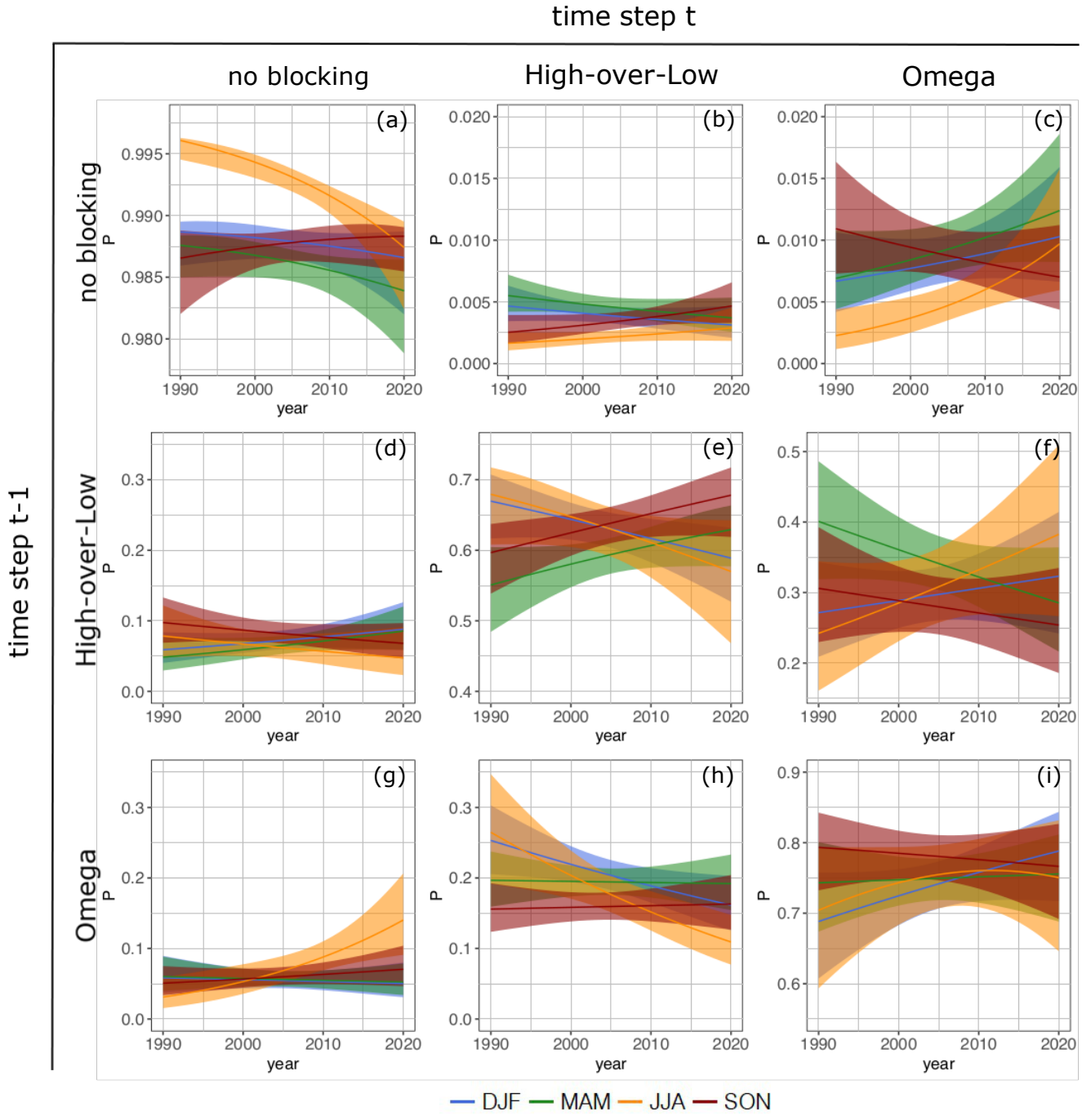

Figure 14. Transition probabilities analogous to the matrix of a three-state Markov process (Eq. 18) as a function of years for individual ~~seasons~~ *seasons* (Eq. 20 and Eq. 21) in the Euro-Atlantic region ($40^\circ\ W - 30^\circ\ E$). Panels are ordered analogously to Fig. 13, season is color coded. Shadings show 95 % confidence intervals.

less likely to evolve into an show a slight decrease in spring and autumn and the opposite transition a slight increase. Although inference is difficult here, these results are consistent with the significant increasing (decreasing) occurrence probability of *Omega* , although these changes are not significant.(*High-over-Low*) blocking in summer and winter (Fig. 10).

5 Summary and Discussion

In this work, we analyse atmospheric blocking probabilities in general and the onset, offset and transition probabilities of blocking in particular. Moreover using a novel method based on the Point vortex theory and the kinematic vorticity number and point vortex theory, we are able to identify and distinguish between two different blocking types: allows to automatically classify atmospheric blocking into *High-over-Low* and *Omega* blocking. The location of the ; the two types are distinguished by the position of the associated low-pressure areas is system(s). These positions are of general importance, as the two different associated blocking types can affect and impact different regions due to their different structures. Using the novel method we can affirm the first question from the introduction, if we can find a method to automatically distinguish between the two different atmospheric blocking types.

In order to estimate the uncertainties of the method, we did a number of experiments depending on different distance criteria for the maximum distance between circulation centroids of successive time steps. The number of identified blocks is sensitive with respect to the distance criterion with lower number for stricter criteria. However, the majority of the experiments agree on the significant results we observe. The main intention to use such a distance criterion is that we want to investigate blocking as a Lagrangian system that we follow in time. The high is assumed to be A key element is the Lagrangian framework, within which we demand the high-pressure system to remain the same vortex over the whole lifetime , but we of the system. We do, however, allow for local variations in and replacements of the low(s). This distinguishes our method and analysis approach from other studies that rather focus on blocking as a large-scale weather regime within a defined region (Eulerian perspective). We thus refine the method developed by Hirt et al. (2015) to identify and distinguish *Omega* and *High-over-Low* blocking. With logistic regression we describe occurrence probabilities for blocking and blocking types and identify potential trends in these broken for individual seasons and months. This is finally extended with Markov models giving additionally transition probabilities between blocked and unblocked states.

As second question, we asked about the occurrence of the different blocking types and if they undergo long-term changes. We further asked if there is a seasonal or even monthly dependence for the different blocking types. By evaluating the occurrence probabilities of the different blocking types we find that the probability of the occurrence of an

5.1 Discussing the two-state model

Investigating blocking without the distinction of *Omega* blocking is higher than that of a and *High-over-Low*, see Fig. 9. In the we see a slight increase of annual occurrence probability in both regions (Fig. 7, black lines). A low probability of blocking in the summer months in the Euro-Atlantic region, the majority of blocks occur in the transitional seasons spring, autumn and in winter for both blocking types (Figs.9b, 10, 11). However, their trends are partly contrary: For example we see significant

~~increases of *Omega* probabilities in summer and winter, but a decrease in autumn in the 30-year period. On the other hand, the probability of *High-over-Low* blocks decreases significantly in winter and summer and increase in autumn (Fig. 10). We can refine this results considering months : While in July *Omega* blocks account for only about 25% of all observed blocks in 1990, we find on the one hand an increase in the number of blocks in general as well as a higher fraction of *Omega* blocks towards the end of the study period. In 2019, the *Omega* blocks pose about 80% of all blocking. Interestingly this relation is reversed in September where the *High-over-Low*s constitute about 20% of all blocking in 1990 vs. about 55% in 2019. It is not clear, why there is a change in the distribution of blocking types. Future studies are challenged to look for changes in e.g. dynamical processes in this time period that might cause these differences.~~

~~In summer, especially in August, the probability of blocking is the smallest. This~~ sector is clearly recognizable. Tyrlis and Hoskins (2008) and Brunner et al. (2017) show similar results regarding the blocking minimum in summer. This minimum can be explained by the variation of the pressure anomalies. In spring and autumn the amplitudes of the pressure anomalies are larger than in summer (see, e.g. Wallace et al., 1993). Therefore, the ~~high and low pressure~~ high- and low-pressure systems are more distinct and can last longer. ~~In Fig. 7b the blocking occurrence probabilities split to seasons are illustrated, where the low probability of blocking in the summer months in the~~ Allowing for different trends in each season reveals increasing trends in occurrence probabilities in summer and winter and decreasing trends in the transition seasons for the larger region (90°W−90°E). These opposing trends add up to the slight increase for the full year. In the Euro-Atlantic ~~sector is clearly recognizable. Tyrlis and Hoskins (2008) and Brunner et al. (2017) show similar results regarding the blocking minimum in summer. But as shown in Fig. 7b the probabilities of blocks slightly, but significantly increase in summer . Therefore,~~ region we see an increase in spring and summer and weaker trends for the other seasons, again summing up to a weak trend for the full year (Fig. 7, colored lines). This difference among the two regions implies that the seasonal dependence of trends varies regionally. The increasing blocking trends in summer support the authors's perception that occurrences of exceptional droughts, that were experienced 2018 and 2019 in central Europe (Hari et al., 2020)~~could occur more often in the future.~~

~~Furthermore, over the 30 year period we observe a strong increase of blocked periods in February and March~~ , are likely to occur more frequently at the end of our study period than at the beginning. A further break down to individual months for the Euro-Atlantic region, reveals that an investigation of trends for a season is not necessarily the best choice to identify changes. While in summer, the trends in occurrence probability are all positive (adding up to a strong positive summer trend), monthly resolved trends in winter, spring and autumn are not in agreement and weaken the seasonal signal (Fig. 8). ~~These~~ Particularly the late winter/early spring (February/March) blocks can have a significant impact on the vegetation and on agriculture in general since they are often connected to temperature extremes. For example, Brunner et al. (2017) found a strong link between cold spell days in February and co-occurrence of blocking, and a link between warm spell days and blocking in late spring in Europe, but they found ~~*no apparent trend in the number of blocked days*~~"no apparent trend in the number of blocked days". However, their study ~~focus laid~~ focused on temperature extremes and not on blocking trends and their identification method differed from ours. Nonetheless, we find a significant increase of blocking occurrence probability in February and March.

In their work on observed blocking trends during the time period 1980–2012, Barnes et al. (2014) ~~did not find a *clear hemispheric increase in blocking* that *is evident in any season for any blocking index, although robust seasonal increases and*~~

~~*decreases are found for isolated regions.*~~ found: "No clear hemispheric increase in blocking is evident in any season for any blocking index, although robust seasonal increases and decreases are found for isolated regions". We can partly confirm this statement: although we find significant trends regarding the seasons, these trends are small and depend on the region. ~~For example the general increase in summer in the Euro-Atlantic region is only in the order of 4 percent points.While spring blocks increase in the Euro-Atlantic region, they decrease in the larger region from 90° *W* to 90° *E*.However, adding more detail to the analysis by considering blocking typesand months leads to significant and stronger trends in some months.However, it should be kept in mind that this further division of the data set leads to smaller samples.~~

~~Fig.12bshows that~~

5.2 Discussing the three-state model

Distinguishing between *Omega* ~~blocks are more persistent than~~ and *High-over-Low* ~~blocks. Furthermore, the formation or onset probability of an~~ blocking, we find occurrence probabilities of *Omega* ~~block is higher than that of a *High-over-Low* blocking . And the transition probability from the~~ blocking being larger than of *High-over-Low* ~~state to the~~ (Figs. 9, 10 and 11). Both types exhibit a different trend in annual occurrence probabilities. While the occurrence probability of *High-over-Low* blocking remains about constant in the study period, a slight increase can be seen for *Omega* ~~block is 0.3, whereas the transition probability from a~~ blocking (Fig. 10, black lines). Resolving these trends seasonally, amplifies the difference between the two types: While occurrence probabilities for *High-over-Low* ~~to an~~ show a slight decrease in summer and winter and increase in the transition seasons (Fig. 10 (a), colors), occurrence probabilities for *Omega* decrease only in autumn and increase in the other seasons, leading to an overall increase (Fig. 10 (b), colors). A further break down of trends for individual months allows for an even more detailed investigation: within one season, the monthly resolved trends do not necessarily agree, as we found for the two-state model. The three-state model now reveals whether a specific type is contributing to changes in blocking occurrence probability or if there are opposing changes for both types leading to minor or no change in overall blocking. Strong trends can be observed for *Omega* blocking occurrence probability for all three winter months, decreasing in December and increasing in January and February; trends are weaker for *High-over-Low* and even ~~*Omega*~~*opposing* ~~block is considerably smaller (0.18). Analysing composites of the blocking onset in the time period June to August, Drouard and Woollings (2018) found that Western- and Central Europe are dominated by a~~ in January (Fig. 11(a)). In spring, monthly resolved trends agree among both types, especially on the increasing trend in March. This reflects the overall blocking trends given in Fig. 8(b) and the seasonal type-specific trends in Fig. 10. Trends in July disagree for *Omega* and *High-over-Low*~~pattern while they found dominating *Omega* pattern for East Europe east of 35° *E*. In order to compare their results with our work, we plotted the total number of blocked time steps with respect to the blocking types and longitudes of occurrence~~ , with the latter decreasing. This results in the small change (non-significant) for overall blocking shown in Fig.~~15. In general, we observe more *Omega* blocks (about 2/3)than *High-over-Low*s (about 1/3) . However, we observe that the share of *High-over-Low*s in~~ 8(c). In autumn, we see strong and opposing trends in September and weak opposing trends in November (Fig. 11(d)). Both lead to (almost) vanishing trends for overall blocking (Fig. 8). For October, both types behave consistent with overall blocking. In some cases, we have thus seen the necessity to be able to distinguish blocking types and also to model trends for individual months.

Otherwise, we would – in some cases – remain with the impression of (almost) constant blocking occurrence probabilities as shown in Figs. 7 and 8 for some seasons or months. The description of type-specific and monthly-resolved trends suggested here is important. Particularly as the location of the ~~total number of blocked time steps is highest between about 0° – 40°E and between about 60°E – 75°E. The fraction of *Omega* blocks is highest for longitudes west of 25°W and for a the region between about 40°E – 60°E. This is comparable to the results of Drouard and Wollings (2018) for their regions between 0°-55°. Their composites for the areas of Western-south central Europe (0–20°E, 40–50°N); Central Europe (20–40°E, 50–60°N) and Western Russia (35–55°E,45-55°N) indeed showed rather *High-over-Low* patterns for the first two regions and an *Omega* pattern for Western Russia. However, our analysis in Fig. 15 is based on the whole year, while Drouard and Woollings (2018) looked at the summer months June to August. Number of total blocked time steps for *Omega* and *High-over-Low* blocks (columns) and percentage of *Omega* (solid red line)/*High-over-Low* (dashed red line) blocks with respect to total blocked time steps. Note that this analysis is based on all blocked time steps in the period 1990-2019. No distinction has been made between season or onset/offset.~~ associated lows differ between types and thus do their impact. Hence with respect to warm and cold spells in early spring and for heatwaves in summer, this distinction between the blocking type is especially relevant to society and should be studied further.

However, adding more detail to the analysis by considering blocking types and individual months leads on the one hand to larger uncertainties as more model parameters are needed to be estimated but on the other hand, this might also lead to stronger signals making statistical significant results possible.

~~The general transition of the two states *no blocking* and *blocking* in Fig. 12a shows that~~

5.3 Discussing transition probabilities for the two-state model

Within the two-state model, the probability of ~~a block remaining blocked~~ remaining in a *blocked* state for the next 6 hours is ~~0.94.The probability of the onset~~ $p_{B,B} = 0.94$ (Table 2, and written at the associated arrows in Fig. 12(a)). The onset probability, i.e.~~the transition probability~~ the transition from the state ~~*no blocking*~~*no-blocking* to ~~the state~~ *blocking*, is much lower (~~about 1%)than~~ $p_{nB,B} \approx 0.01$), so is the offset probability ~~(about 6%), because there are more time steps unblocked than blocked. In comparison,~~ $p_{B,nB} \approx 0.06$. Spekat et al. (1983) found daily transition probabilities for the onset of a meridional weather regime of 8% (zonal→meridional) to 11% (mixed state→meridional) and high probabilities to stay within the same weather regime (between 0.81 and 0.86). Their offset probabilities range from 5% (meridional→zonal) to 9% (meridional→mixed state). Their onset values are comparable to our results if we ~~downscale~~ upscale the 6-hourly data to daily time steps. Moreover, we can confirm that the probability is higher to remain within the same state. ~~A~~ We refrain from a more detailed comparison ~~is complicated, because~~ as their method differs in many respects from the one we use. While Spekat et al. (1983) uses a large-scale weather regime classification, our method is based on the identification of the blocking pattern itself and is rather event-based.

~~Finally, we tackle the third question asked in the introduction: Are there trends in the transition of different blocking types and do these transitions depend on the season, or even on the month? The results of the transitions~~ Trends in the transition probabilities for the two-state model ~~and the three-state model does not show significant trends on a yearly analysis~~ are not

significant (see Supplementary Material~~Fig. .~~ Figs. S.8 and ~~Fig. 13). But the further split into the seasonal temporal evolution shows a significant trend of the onset and offset of~~ S.9). This is different for some of the observed trends in the three-state model.

5.4 Discussing transition probabilities for the three-state model

The transition probabilities for the three-state model (Table 3, and written at the associated arrows in Fig. 12(b)) show that i) *Omega* ~~blocks during the summer months, see Fig.14c, g. The conversion from an~~ blocks are more persistent than *High-over-Low* blocks, ii) blocking formation or onset is more likely to start with *Omega* ~~block to a~~ than with *High-over-Low* ~~decreases (Fig. 14h).~~ blocking, and iii) the transition probability from *High-over-Low* to *Omega* $p_{HoL,\Omega} = 0.3$ is almost 1.5 times larger than the probability for the opposite transition ($p_{HoL,\Omega} = 0.18$). This suggests that the *Omega* blocking is more stable and more likely to onset than *High-over-Low*. It is unclear, why *Omega* blocking are more stable than *High-over-Low* blocks. Lucarini et al. (2016) finds that blocking periods, in general, are characterized by higher instability than unblocked flows. This might also justify the occurrence of blocking type changes from *High-over-Low* to *Omega* and vice versa. Additionally, the authors speculate that a vortex configuration of three vortices is more stable and less disturbed by other vortices embedded in the jet, but this needs to be studied further before a clear answer can be given.

~~We remark that the outcomes depend on the methods and on the time resolution. Using data with a 6 hourly time resolution , we obtain~~ The likelihood-ratio test suggests a significant improvement when including the covariate Years to describe a trend. However, the large confidence intervals in Fig. 13 do not allow a detailed interpretation of individual transition probabilities other than those conditioned on the *no-blocking* state (first row). Estimating these trends in transition probabilities individually for every season leads to a more complex model with more parameters and thus larger confidence intervals, see Fig. 14. However, this model now reveals stronger signals which are in part opposing and thus superimpose to the weaker signals we see in Fig. 13. Particularly interesting are the trends found in summer as described in Sec. 4.4.2. Again, the complex model allowing for two blocking types and for different trends in each seasons is necessary to reveal signals which otherwise average out.

5.5 Discussion of the method

Characterizing blocking and blocking types is to a large degree dependent on time resolution and methods. The 6-hourly time resolution yields a larger data basis compared to ~~data based on daily means. Regarding the methods, the blocked time steps are initially identified with the help of the~~ daily means, but potentially contains also more uninteresting variability (noise). Our identification and classification strategy starts with the well accepted instantaneous blocked longitudes (IBL) ~~method~~ after Tibaldi and Molteni (1990), see also Richling et al. (2015). ~~The identification~~ However, the subsequent algorithm (Step 1-4, ~~Section~~ Sec. 3, see also Fig. 2) is ~~based on many assumptionsand not flawless. The IBL method is a one-dimensional method. Although we applied a seasonally varying reference latitude , a one-dimensional method might have problems in detecting blocked situations properly. Especially, the thresholds of northern and southern~~ complex and requires many assumptions. Critical can be the choice of the reference latitude (seasonally-varying vs. annual) and the fixed thresholds for the geopotential

height gradients~~are fixed values and applied for the whole year~~. This might explain why there are fewer blocks detected in summer~~. See also~~, see also, e.g. Scherrer et al. (2006), who show that the frequency of blocks is strongly dependent on the reference latitude. ~~Moreover, the choice of the investigated domain can have an impact on the results, see e.g. Fig. 7. We also note that the data assimilation techniques as well as the amount of observational data assimilated did change over the years, which can lead to slightly inhomogeneous data. This might further obscure real trends from artificial ones (Sterl, 2004). Since our study regions are in the northern hemispheric mid-latitudes and our period lies in the post-satellite era, we expect the data to be relative homogeneous. We also choose five days (=20 time steps) as a minimum duration for our definition of blocking in the larger domain. Although we made a subset of the larger domain and the length of stay within the smaller Euro-Atlantic sector can be smaller than 5 days, the minimum lifetime of the associated block period is still 5 days. However, changing this minimum duration~~ Changing the minimum duration criterion leads to a higher or lower number of identified blocks. Furthermore, the results can depend on the specific blocking identification method used, the region and season (Pinheiro et al., 2019): Investigating the blocking identification methods based on the vertically averaged potential vorticity anomaly (Schwierz et al., 2004), the geopotential height anomaly (Dole and Gordon, 1983), and geopotential height gradient after Tibaldi and Molteni (1990) that is applied here, Pinheiro et al. (2019) found that ~~*each of the three algorithms produce distinct regional and seasonal differences in their overall global blocking climatology*~~"each of the three algorithms produce distinct regional and seasonal differences in their overall global blocking climatology". Moreover, the decision between *High-over-Low* and *Omega* blocking types is based on a comparison of the vortex field south of the high center. The vortex field is inspected in a box with a width of 25 degrees longitudes directly below the high and compared to the two neighboring boxes (see Fig. 3). A change in the box width obviously can affect the ~~percentage~~ fraction of identified *High-over-Low*s vs. *Omega* blocks. In our setting, the method identifies about 2/3 of all blocking as *Omega* types. However, ~~this changes~~ using a different box width might change the ratio of identified *Omega* vs. *High-over-Low* blocks, but does not explain the partially contrary trends we observe in their probability in some months such as the increase of *Omega* blocks in summer while the *High-over-Lows* decrease. These must stem from another mechanism, ~~maybe~~ such as a change in the underlying large-scale flow or the position or strength of the jet ~~. Furthermore, changing the region of interest (Step 4 in Section 3) can lead to different results than previous works. A~~ (Woollings and Blackburn, 2012).

However, we want to point out that a major benefit of ~~this approach based on the kinematic vorticity number~~ our method is the identification and location of each single vortex – the ~~high pressure~~ high-pressure area as well as the one or two ~~low pressure~~ low-pressure areas – forming the *High-over-Low*, respectively the *Omega* block.

6 ~~Conclusion~~

~~Using logistic regression and the Markov model, we investigate onset, offset and transition probabilities of atmospheric blocking during~~ This allows to distinguish between the blocking types within and for each single blocking period, separately. This gives more detail compared to averaging over multiple blocking periods as is typically done to derive composites. E.g., analysing composites of the blocking onset in the time period ~~1990-2019 in the Euro-Atlantic sector (40°W-30°E) and for the~~

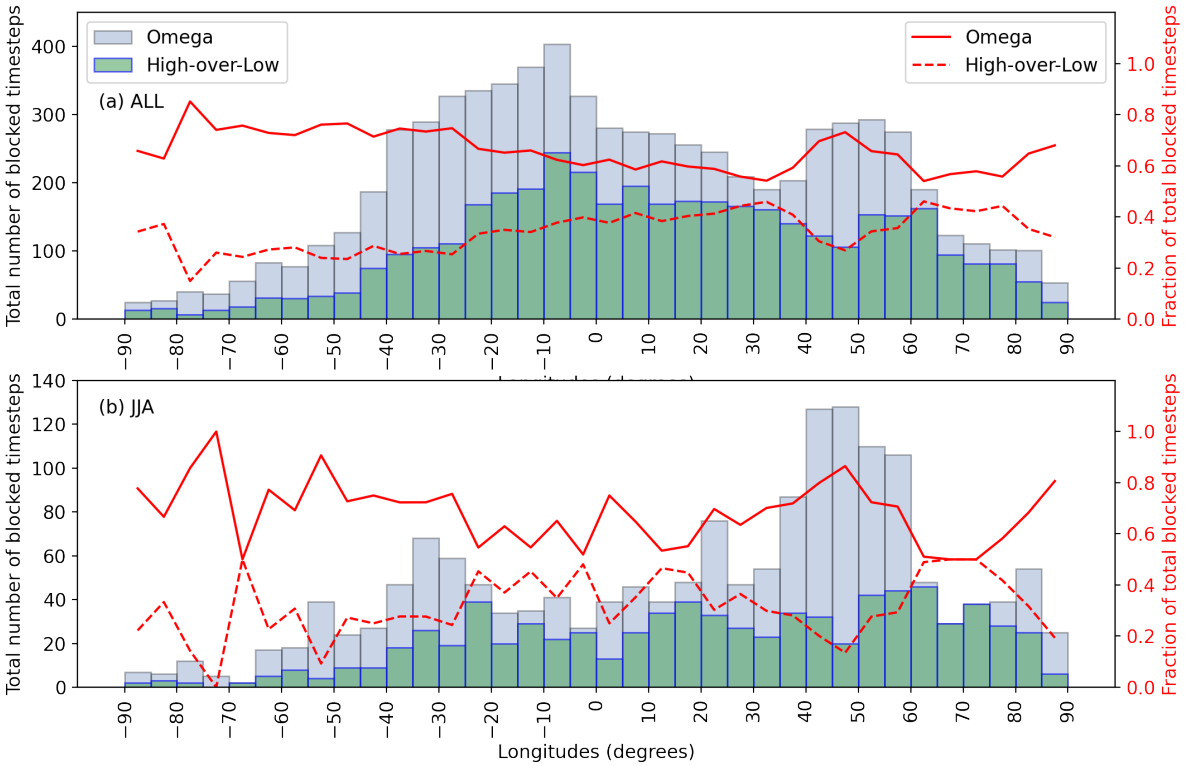

Figure 15. Number of total blocked time steps for *Omega* and *High-over-Low* blocks (columns) and percentage of *Omega* (solid red line)/*High-over-Low* (dashed red line) blocks with respect to total blocked time steps. Note that this analysis is based on (a) all blocked time steps and (b) blocked time steps in JJA in the period 1990-2019. No distinction has been made between onset or offset.

~~larger region (90°W-90°E). In the following, we will summarize our main results~~ June to August, Drouard and Woollings (2018) found that Western- and Central Europe are dominated by a *High-over-Low* pattern while they found dominating *Omega* patterns for East Europe east of 35° E. In order to compare (and complement) their results to our work, we plot the total number of blocked time steps with respect to the ~~three research questions posed in the introduction:~~

~~Can we find a method to automatically distinguish between the two atmospheric blocking types~~ blocking types and longitudes of occurrence in Fig. 15. In general, we observe more *Omega* blocks (about 2/3) than *High-over-Low*~~and~~s (about 1/3). The share of *High-over-Low*s of total number of blocked time steps is largest between about 0° – 40°E and between about 60°E–75°E for the whole year (Fig. 15(a)). The western region with a large fraction of *High-over-Low*s is shifted to the west in summer to 25°W–20°E and the eastern region 60°E–75°E shows an even higher fraction of about 1/2 (Fig. 15(b)). The fraction of *Omega* blocks ~~?~~

~~To tackle this first question, we introduced a blocking type decision method based on the kinematic vorticity number and point vortex principles,that identifies~~ is highest for longitudes west of 25°W and for a the region between about 40°E–60°E. In summer the contrast in western Russia is even more pronounced with a maximum of about 80% *Omega* blocks compared to the whole year. This is comparable to the results of Drouard and Woollings (2018) for their regions between 0°-55°E. Their composites for the western area (south-central Europe) (0–20°E, 40–50°N); central area (20–40°E, 50–60°N) and Western Russia (35–55°E,45-55°N) indeed showed rather *High-over-Low* ~~and~~ patterns for the first two regions and an *Omega* ~~patterns for each blocked time step, separately.~~ pattern for Western Russia.

6 Conclusion

Blocked weather situations are usually analysed with respect to the persistent high ~~, which~~ pressure system. This quasi-stationary high can for example lead to droughts with devastating consequences. ~~Using the point vortex theory, we require the sum of the circulations of the high and low pressure areas to be zero. The additional consideration of the low~~Here, we additionally consider the position(s) of the low pressure system(s) in a blocking identification method. This is a novelty and provides the possibilities for further studies, for example on the impact of the steady ~~low pressure~~ low-pressure systems such as heavy rainfall and ~~floods.~~ flooding events.

This novel strategy is based on point vortex theory to identify and classify blocking. Combined with logistic regression and Markov processes, this allows a fresh view on blocking occurrence and transition dynamics. We consider the time period 1990-2019 in the Euro-Atlantic sector (40°W-30°E) and for a larger region on the Northern Hemisphere (90°W-90°E). A blocking type identification method based on the kinematic vorticity number and point vortex principles classifies *High-over-Low* and *Omega* patterns for each blocked time step, separately. This method was developed by Hirt et al. (2018) and refined in this paper. In general, we observe that about 2/3 of all blocks are *Omega* blocks and about 1/3 are *High-over-Low* blocks, although this fractions can vary with longitude, season and year (Figs. 9, 15).

~~(2) Do blocking occurrence probabilities undergo long-term changes? Do these changes depend on the season or month?~~

Conclusion with respect to the two research questions posed in the introduction are given in the following.

~~For both regions, we observe only small significant changes in the yearly and seasonal blocking frequency over the 30 year period. But, we observe large significant increases in the blocking probability for some months, especially February and March. We observe a steady, but slight increase for the summer months, too.In addition, a strong significant decrease is observed in December over the 30 years. These changes can be attributed predominantly to *Omega* blocks (Figs. 7, 8, 10, 11).~~

~~(3) Do onset (formation), offset (decay) or transition probabilities from one blocking type to another undergo~~

1. **Do blocking occurrence probabilities undergo long-term changes? Do these changes depend on the season or month?**

   It turns out, that for the time period under investigation, trends in annual blocking occurrence probabilities are small

compared to their long-term ~~changes? Do these changes depend on season or month? In order to answer this third question, we use a Markov model to calculate transition probabilitiesof the different blocking types *High-over-Low* and~~ averages. The analysis of seasonal occurrence probabilities reveals that stronger but partly opposing seasonal trends exist; these, however, averaged over seasons, exhibit the observed weak annual signal. A similar effect emerges when breaking trends down to monthly occurrence probabilities. Particularly for winter and spring, individual months (February and March) show strong trends which are opposing the trends in other month of the same season. On the one hand, this highlights problems associated with aggregating time series and on the other hand reveals changes in blocking occurrence in late winter and early spring with potential impact on vegetation and agriculture, which would have been hidden otherwise. The key element of this study – the distinction between *Omega* ~~blocking and of the state *no blocking*. We show that *Omega* blocking is more likely to occur and more persistent than the~~ and *High-over-Low* ~~blocking pattern (Fig. 12) . Regarding the seasons over the 30 year period, we found the largest changes in transition probabilities in the summer season, where the transition probability to *Omega* blocks increase strongly, while the *unblocked* state becomes less probable. Hence, *Omega* blocks become more frequent and stable in summer. Moreover, we observe a higher probability for the transition from *High-over-Low* to *Omega* blocks in the summer season towards the end of the study period (cf. Fig. 14). This confirms the impression that~~ – allows to break down the monthly resolved trends to the two types. This reveals different magnitudes (December, February) and opposing trends (January, July, September). This information is potentially relevant for weather impact related to the different locations of the low-pressure systems associated with the two blocking types. Furthermore, we can now state that i) blocking in summer has become more prominent in recent years over the European ~~continents~~continent and ii) this is due to a strong increase in *Omega* blocking which cannot be set off by a slight decrease of *High-over-Low*. Additionally, ~~we show that this increase in summer blocking is explained by~~ this distinction is an interesting starting point for further research on blocking mechanisms; a first small step in this direction provide Markov models to describe onset and decay of as well as transitions between the blocking types.

2. Do onset (formation), offset (decay) or transition probabilities from one blocking type to another undergo long-term changes? Do these changes depend on season or month?

Trends in annual transition probabilities show an increase in the onset of *Omega* ~~blocking patterns.~~

~~In future studies, for a deeper understanding of atmospheric blocking, the relation of on- and offset of blocking~~ patterns; other annual transition probabilities have confidence intervals being compatible with constant values and should be interpreted with care. Again, a break down into monthly resolved trends gives more robust results and shows once more opposing trends for different seasons which are the reason for the weak annual signals. Most prominent are trends in summer with an increase in onset to *Omega* and an increase in transition from *High-over-Low* to ~~different parameters such as NAO,~~ *Omega* accompanied with a decrease in the opposite direction; persistence of *Omega* increases until about 2010 and stagnates thereafter, accompanied with a slight decay of the latter.

Our strategy to distinguish *Omega* and *High-over-Low* blocking with subsequent logistic regression involving Markov models can provide the basis for future studies to investigate the dependence of onset and decay of blocking on, e.g., the

~~temperature, or the wind shear should be investigated~~North-Atlantic-Oscillation (NAO) index, temporal gradients in mid-latitude wind speeds or the speed and location of the jet that could influence the blocking process in Europe, see e.g. Luo et al. (2019) or Riboldi et al. (2020) who show that periods of reduced Rossby wave phase speed are systematically related to atmospheric blocking.

Additionally, diabatic effects such as latent heat release play an important role in blocking dynamics (Pfahl et al., 2015; Steinfeld and Pfa
. Thus, studying this relation with respect to different blocking types might be insightful. Moreover, the authors suggest to ~~either add a tracking method~~ identify blocking by means of identifying and tracking the associated vortices additionally to the blocking identification ~~process or substitute the blocking identification~~ based on indices~~to a vortex identification method~~. This can be achieved, for example, based on the kinematic vorticity number (Schielicke et al., 2016). ~~However, since the here introduced method can identify the high pressure area *and* the low pressure area, it can further be used for novel statistical evaluations of extreme events caused by lows, as for example floods. Our results indicate rather monthly and more local changes of atmospheric blocks which underlines the necessity to analyse persistent high and low pressure areas separately. We~~

We finally conclude, that ~~the use of logistic regression and the combination~~ distinguishing blocking types and describing their occurrence and transition probabilities with logistic regression combined with Markov models ~~with two and three possible states for different blocking types~~ gives valuable insight into the ~~development~~ dynamics of atmospheric blocking ~~especially when analysing the changes for seasons or individual months~~and their changes for Euro-Atlantic and potentially also for other regions.

Author contributions. A.M., P.N. and H.R. designed the study. C.D. did the statistical analysis and visualised the results, mainly at the FU Berlin. L.S. wrote and adapted the trapezoid method and blocking type decision method and performed further uncertainty experiments. H.R. and C.D. wrote the statistical chapters and discussed the related results. C.D., H.R., A.M. and L.S. continuously wrote on the paper draft and discussed the results. All authors discussed and finalised together the paper.

Competing interests. The authors declare that no competing interests are present.

Code and data availability. The NCEP-DOE Reanalysis 2 data that supports the findings of this study is available via rda.ucar.edu with the identifier DOI:10.5065/KVQZ-YJ93. All code can be provided upon request.

Acknowledgements. We thank I. Kröner for critical discussions and reading the manuscript. We would like to thank two anonymous reviewers for their input, questions and comments that helped improving this work! Moreover, we thank George Pacey and Edmund Meredith for helpful comments. This research has been partially funded by Deutsche Forschungsgemeinschaft (DFG) through grant CRC 1114 'Scaling

Cascades in Complex Systems, Project Number 235221301, Projects A01 'Coupling a multiscale stochastic precipitation model to large scale atmospheric flow dynamics' and C06 'Multiscale structure of atmospheric vortices'.

References

Altenhoff, A. M., Martius, O., Croci-Maspoli, M., Schwierz, C., and Davies, H. C.: Linkage of atmospheric blocks and synoptic-scale Rossby waves: a climatological analysis, Tellus A, 60, 1053–1063, https://doi.org/10.1111/j.1600-0870.2008.00354.x, 2008.

Aref, H.: Motion of three vortices, Physical Fluids, 22, 1979.

Baclawski, K.: Introduction to probability with R, Chapman & Hall/CRC Texts in statistical science, 2008.

Barnes, E. A., Slingo, J., and Woollings, T.: A methodology for the comparison of blocking climatologies across indices, models and climate scenarios, Clim. Dynam., 38, 2467–2481, https://doi.org/10.1007/s00382-011-1243-6, 2011.

Barnes, E. A., Dunn-Sigouin, E., Masato, G., and Woollings, T.: Exploring recent trends in Northern Hemisphere blocking, Geophys. Res. Lett., 41, 638–644, 2014.

Barriopedro, D., García-Herrera, R., Lupo, A. R., and Hernández, E.: A climatology of Northern Hemisphere blocking, J. Climate, 19, 1042–1063, https://doi.org/10.1175/JCLI3678.1, 2006.

Barriopedro, D., García-Herrera, R., and Trigo, R.: Application of blocking diagnosis methods to general circulation models. Part I: A novel detection scheme, Clim. Dynam., http://link.springer.com/article/10.1007/s00382-010-0767-5, 2010.

Berrisford, P., Hoskins, B. J., and Tyrlis, E.: Blocking and Rossby Wave Breaking on the Dynamical Tropopause in the Southern Hemisphere, J. Atmos. Sci., 64, 2881–2898, https://doi.org/10.1175/JAS3984.1, 2007.

Bissolli, P., Deutschländer, T., Imbery, F., Haeseler, S., Lefebvre, C., Blahak, J., Fleckenstein, R., Breyer, J., Rocek, M., Kreienkamp, F., Rösner, S., and Schreiber, K.-J.: Hitzewelle Juli 2019 in Westeuropa – neuer nationaler Rekord in Deutschland, https://www.dwd.de/DE/leistungen/besondereereignisse/temperatur/20190801_hitzerekord_juli2019.pdf?__blob=publicationFile&v=3, Deutscher Wetterdienst, Abteilung Klimaüberwachung. Press release (in German), 1 Aug 2019 (last access: 31 Aug 2020), 2019.

Bott, A.: Synoptische Meteorologie, Springer Berlin Heidelberg, https://doi.org/10.1007/978-3-642-25122-1, 2012.

Brunner, L., Hegerl, G. C., and Steiner, A. K.: Connecting atmospheric blocking to European temperature extremes in spring, J. Climate, 30, 585–594, 2017.

Brunner, L., Schaller, N., Anstey, J., Sillmann, J., and Steiner, A. K.: Dependence of present and future European temperature extremes on the location of atmospheric blocking, Geophys. Res. Lett., 45, 6311–6320, 2018.

Cheung, H. N., Zhou, W., Mok, H. Y., Wu, M. C., and Shao, Y.: Revisiting the climatology of atmospheric blocking in the Northern Hemisphere, Adv. Atmos. Sci., 30, 397–410, 2013.

Davini, P. and D'Andrea, F.: From CMIP3 to CMIP6: Northern Hemisphere atmospheric blocking simulation in present and future climate, J. Climate, 33, 10 021–10 038, 2020.

Davini, P., Cagnazzo, C., Gualdi, S., and Navarra, A.: Bidimensional diagnostics, variability, and trends of Northern Hemisphere blocking, J. Climate, 25, 6496–6509, 2012.

Deutscher Wetterdienst: The weather in Germany in July 2019, https://www.dwd.de/EN/press/press_release/EN/2019/20190730_the_weather_in_germany_in_july_2019.pdf?__blob=publicationFile&v=2, press release, 30 July 2019 (last access: 31 Aug 2020), 2019.

Deutscher Wetterdienst: DWD-Stationen Duisburg-Baerl und Tönisvorst jetzt Spitzenreiter mit 41,2 Grad Celsius, https://www.dwd.de/DE/presse/pressemitteilungen/DE/2020/20201217_annulierung_lingen_news.html, press release, 17 December 2020 (in German, last access: 11 Feb 2021), 2020.

Dobson, A. J. and Barnett, A. G.: An introduction to generalized linear models, Third Edition, Texts in Statistical Science, Chapman & Hall, 2008.

Dole, R. M. and Gordon, N. D.: Persistent anomalies of the extratropical northern hemisphere wintertime circulation: Geographical distribution and regional persistence characteristics, Mon. Weather Rev., 111, 1567–1586, 1983.

Drouard, M. and Woollings, T.: Contrasting mechanisms of summer blocking over western Eurasia, Geophys. Res. Lett., 45, 12–040, 2018.

Egger, J.: The blocking transition, in: Irreversible phenomena and dynamical systems analysis in geosciences, edited by Nicolis, C. and Nicolis, G., pp. 181–197, Springer Netherlands, Dordrecht, https://doi.org/10.1007/978-94-009-4778-8_10, 1987.

Ferranti, L., Corti, S., and Janousek, M.: Flow-dependent verification of the ECMWF ensemble over the Euro-Atlantic sector, Q. J. Roy. Meteor. Soc., 141, 916–924, 2015.

Freva: Freie Universität Berlin evaluation system (Freva), https://freva.met.fu-berlin.de/, accessed: 2020-09-10, 2017.

Gottwald, G. A., Crommelin, D. T., and Franzke, C. L. E.: Stochastic climate theory, arXiv, (last access: 31 Aug 2020), 2016.

Grewal, J. K., Krzywinski, M., and Altman, N.: Markov models – Markov chains, Nat. Methods, 16, 663–664, https://doi.org/10.1038/s41592-019-0476-x, 2019.

Hari, V., Rakovec, O., Markonis, Y., Hanel, M., and Kumar, R.: Increased future occurrences of the exceptional 2018–2019 Central European drought under global warming, Sci. Rep-UK, 10, 1–10, 2020.

Henley, J., Chrisafis, A., and Jones, S.: France records all-time highest temperature of 45.9C, The Guardian, 28 Jun 2019 (last access: 31 Aug 2020), 2019.

Hirt, M., Kröner, I., and Dioni, E.: Numerical simulaton of vortex flows with a meteorological application – Report for the project "Vortex Flows", Tech. rep., Technische Universität Berlin, 2015.

Hirt, M., Schielicke, L., Müller, A., and Névir, P.: Statistics and dynamics of blockings with a point vortex model, Tellus A: Dynamic Meteorology and Oceanography, 70, 1–20, 2018.

Hong, C.-C., Hsu, H.-H., Lin, N.-H., and Chiu, H.: Roles of European blocking and tropical-extratropical interaction in the 2010 Pakistan flooding, Geophys. Res. Lett., 38, 2011.

Kadow, C., Illing, S., Lucio-Eceiza, E. E., Bergemann, M., Ramadoss, M., Sommer, P. S., Kunst, O., Schartner, T., Pankatz, K., Grieger, J., et al.: Introduction to Freva–A Free Evaluation System Framework for Earth System Modeling, Journal of Open Research Software, 9, 2021.

Kanamitsu, M., Ebisuzaki, W., Woollen, J., Yang, S.-K., Hnilo, J., Fiorino, M., and Potter, G.: Ncep–doe amip-ii reanalysis (r-2), B. Am. Meteorol. Soc., 83, 1631–1644, 2002.

Kimoto, M. and Ghil, M.: Multiple flow regimes in the Northern Hemisphere winter. Part II: Sectorial regimes and preferred transitions, J. Atmos. Sci., 50, 2645–2673, 1993.

Kuhlbrodt, T. and Névir, P.: Low-order point vortex models of atmospheric blocking, Meteorology and Atmospheric Physics, 73, 127–138, 2000.

Lucarini, V., Freitas, A. C. M., Nicol, M., Freitas, J. M., Todd, M., Faranda, D., Kuna, T., Hollande, M., and Vaienti, S.: Extremes and recurrence in dynamical systems, Wiley, 2016.

Luo, D., Zhang, W., Zhong, L., and Dai, A.: A nonlinear theory of atmospheric blocking: A potential vorticity gradient view, Journal of Atmospheric Sciences, 76, 2399–2427, 2019.

Markov, A. A.: An Example of Statistical Investigation of the Text Eugene Onegin Concerning the Connection of Samples in Chains, Sci. Context, 19, 591–600, https://doi.org/10.1017/S0269889706001074, 2006.

Matlab: MATLAB version 9.0.0.341360 (R2016a), The MathWorks Inc., Natick, Massachusetts, 2016.

McCullagh, P. and Nelder, J. A.: Generalized Linear Models 2nd edition, London, UK, 1989.

Mohr, S., Wilhelm, J., Wandel, J., Kunz, M., Portmann, R., Punge, H. J., Schmidberger, M., Quinting, J. F., and Grams, C. M.: The role of large-scale dynamics in an exceptional sequence of severe thunderstorms in Europe May–June 2018, Weather and Climate Dynamics, 1, 325–348, https://doi.org/10.5194/wcd-1-325-2020, 2020.

Müller, A. and Névir, P.: A geometric application of Nambu mechanics: the motion of three point vortices in the plane, J. Phys. A-Math. Theor., 47, 105 201, 2014.

Müller, A., Névir, P., Schielicke, L., Hirt, M., Pueltz, J., and Sonntag, I.: Applications of point vortex equilibria: blocking events and the stability of the polar vortex, Tellus A, 67, https://doi.org/10.3402/tellusa.v67.29184, 2015.

Newton, P. K.: The N-Vortex Problem: Analytical Techniques, Springer-Verlag, 2001.

Obukhov, A., Kurganskii, M., and Tatarskaia, M.: Dynamic conditions for the origin of drought and other large-scale weather anomalies, Meteorologiia i Gidrologiia, pp. 5–13, 1984.

Pelly, J. L. and Hoskins, B. J.: A new perspective on blocking, J. Atmos. Sci., 60, 743–755, 2003.

Pfahl, S. and Wernli, H.: Quantifying the relevance of atmospheric blocking for co-located temperature extremes in the Northern Hemisphere on (sub-) daily time scales, Geophys. Res. Lett., 39, 2012.

Pfahl, S., Schwierz, C., Croci-Maspoli, M., Grams, C. M., and Wernli, H.: Importance of latent heat release in ascending air streams for atmospheric blocking, Nature Geoscience, 8, 610–614, 2015.

Pinheiro, M., Ullrich, P., and Grotjahn, R.: Atmospheric blocking and intercomparison of objective detection methods: flow field characteristics, Clim. Dynam., 53, 4189–4216, 2019.

R Core Team: R: A language and environment for statistical computing, R Foundation for Statistical Computing, Vienna, Austria, https://www.R-project.org/, 2018.

Rex, D. F.: Blocking action in the middle troposphere and its effect upon regional climate: Part I. An aerological study of blocking action, Tellus, 2, 196–211, 1950.

Riboldi, J., Lott, F., d'Andrea, F., and Rivière, G.: On the Linkage Between Rossby Wave Phase Speed, Atmospheric Blocking, and Arctic Amplification, Geophysical Research Letters, 47, e2020GL087 796, 2020.

Richling, A., Kadow, C., Illing, S., and Kunst, O.: Freie Universität Berlin evaluation system (Freva) - Blocking, https://freva.met.fu-berlin.de/about/blocking/, (Documentation of the blocking plugin), Accessed: 2020-09-10, 2015.

Russo, S., Sillmann, J., and Fischer, E. M.: Top ten European heatwaves since 1950 and their occurrence in the coming decades, Environ. Res. Lett., 10, 2015.

Scherrer, S. C., Croci-Maspoli, M., Schwierz, C., and Appenzeller, C.: Two-dimensional indices of atmospheric blocking and their statistical relationship with winter climate patterns in the Euro-Atlantic region, Int. J. Climatol., 26, 233–249, 2006.

Schielicke, L.: Scale-dependent identification and statistical analysis of atmospheric vortex structures in theory, model and observation, Ph.D. thesis, Freie Universität Berlin, Berlin, Germany, 2017.

Schielicke, L., Névir, P., and Ulbrich, U.: Kinematic vorticity number – a tool for estimating vortex sizes and circulations, Tellus A, 68, https://doi.org/10.3402/tellusa.v68.29464, 2016.

Schneidereit, A., Schubert, S., Vargin, P., Lunkeit, F., Zhu, X., Peters, D., and Fraedrich, K.: Large-Scale Flow and the Long-Lasting Blocking High over Russia: Summer 2010, Monthly Weather Review, 140, 2967–2981, https://doi.org/10.1175/MWR-D-11-00249.1, 2012.

Schwierz, C., Croci-Maspoli, M., and Davies, H.: Perspicacious indicators of atmospheric blocking, Geophys. Res. Lett., 31, 2004.

Spekat, A., Heller-Schulze, B., and Lutz, M.: Über Großwetterlagen und Markov-Ketten, Meteorol. Rundsch., 36, 243–248, in German, 1983.

Steinfeld, D. and Pfahl, S.: The role of latent heating in atmospheric blocking dynamics: a global climatology, Climate Dynamics, 53, 6159–6180, 2019.

Sterl, A.: On the (in) homogeneity of reanalysis products, J. Climate, 17, 3866–3873, 2004.

Tibaldi, S. and Molteni, F.: On the operational predictability of blocking, Tellus A, 42, 343–365, https://doi.org/10.1034/j.1600-0870.1990.t01-2-00003.x, 1990.

Truesdell, C.: Two measures of vorticity, Indiana Univ. Math. J., 2, 173–217, 1953.

Truesdell, C.: The kinematics of vorticity, Indiana University Press, Bloomington, Indiana, 1954.

Tung, K. K. and Lindzen, R.: A theory of stationary long waves. Part I: A simple theory of blocking, Mon. Weather Rev., 107, 714–734, 1979.

Tyrlis, E. and Hoskins, B. J.: Aspects of a northern hemisphere atmospheric blocking Climatology, J. Atmos. Sci., 65, 1638–1652, https://doi.org/10.1175/2007JAS2337.1, 2008.

Vautard, R., Mo, K. C., and Ghil, M.: Statistical significance test for transition matrices of atmospheric Markov chains, J. Atmos. Sci., 47, 1926–1931, 1990.

Vautard, R., van Aalst, M., Boucher, O., Drouin, A., Haustein, K., Kreienkamp, F., Van Oldenborgh, G. J., Otto, F. E., Ribes, A., Robin, Y., et al.: Human contribution to the record-breaking June and July 2019 heatwaves in Western Europe, Environmental Research Letters, 15, 094 077, 2020.

Wallace, J. M., Zhang, Y., and Lau, K.-H.: Structure and seasonality of interannual and interdecadal variability of the geopotential height and temperature fields in the Northern Hemisphere troposphere, J. Climate, 6, 2063–2082, 1993.

Wilks, D. S.: Statistical methods in the atmospheric sciences, vol. 100 of *International geophysics series*, Academic Press, 3 edn., 2011.

Woollings, T. and Blackburn, M.: The North Atlantic jet stream under climate change and its relation to the NAO and EA patterns, Journal of Climate, 25, 886–902, 2012.

Woollings, T., Barriopedro, D., Methven, J., Son, S.-W., Martius, O., Harvey, B., Sillmann, J., Lupo, A. R., and Seneviratne, S.: Blocking and its response to climate change, Current climate change reports, 4, 287–300, 2018.

Yee, T. W.: Vector generalized linear and additive models: With an implementation in R, Springer, New York, USA, 2015.